

Combination of electroweak and QCD corrections to single W production at the Fermilab Tevatron and the CERN LHC

Giovanni Balossini and Guido Montagna

Dipartimento di Fisica Nucleare e Teorica, Università di Pavia, and INFN, Sezione di Pavia, via A. Bassi 6, 27100 Pavia, Italy
Email: giovanni.balossini@pv.infn.it
Email: guido.montagna@pv.infn.it

Carlo Michel Carloni Calame

Istituto Nazionale di Fisica Nucleare, Via E. Fermi 40, Frascati, Italy
and School of Physics & Astronomy, University of Southampton, Highfield, Southampton SO17 1BJ, UK
Email: c.carloni-calame@phys.soton.ac.uk

Mauro Moretti

Dipartimento di Fisica, Università di Ferrara, and INFN, Sezione di Ferrara, via Saragat 1, 44100 Ferrara, Italy
Email: mauro.moretti@fe.infn.it

Oreste Nicosini and Fulvio Piccinini

INFN, Sezione di Pavia, via A. Bassi 6, 27100 Pavia, Italy
Email: oreste.nicosini@pv.infn.it
Email: fulvio.piccinini@pv.infn.it

Michele Treccani

Departamento de Física Teórica y del Cosmos, CAPFE, Universidad de Granada, Avenida de Fuentenueva, E-18071 Granada, Spain
Email: treccani@ugr.es

Alessandro Vicini

Dipartimento di Fisica, Università di Milano, and INFN, Sezione di Milano, Via Celoria 16, 20133 Milano, Italy
Email: alessandro.vicini@mi.infn.it

ABSTRACT: Precision studies of the production of a high-transverse momentum lepton in association with missing energy at hadron colliders require that electroweak and QCD higher-order contributions are simultaneously taken into account in theoretical predictions and data analysis. Here we present a detailed phenomenological study of the impact of electroweak and strong contributions, as well as of their combination, to all the observables relevant for the various facets of the $pp^{(-)} \rightarrow \text{lepton} + X$ physics programme at hadron colliders, including luminosity monitoring and Parton Distribution Functions constraint, W precision physics and search for new physics signals. We provide a theoretical recipe to carefully combine electroweak and strong corrections, that are mandatory in view of the challenging experimental accuracy already reached at the Fermilab Tevatron and aimed at the CERN LHC, and discuss the uncertainty inherent the combination. We conclude that the theoretical accuracy of our calculation can be conservatively estimated to be about 2% for standard event selections at the Tevatron and the LHC, and about 5% in the very high W transverse mass/lepton transverse momentum tails. We also provide arguments for a more aggressive error estimate (about 1% and 3%, respectively) and conclude that in order to attain a one per cent accuracy: 1) exact mixed $\mathcal{O}(\alpha\alpha_s)$ corrections should be computed in addition to the already available NNLO QCD contributions and two-loop electroweak Sudakov logarithms; 2) QCD and electroweak corrections should be coherently included into a single event generator.

KEYWORDS: Hadronic Colliders; Standard Model; QCD.

Contents

1. Introduction	1
2. Theoretical ingredients	4
2.1 Parton Distribution Functions (PDF)	4
2.2 QCD corrections and Monte Carlo tools	5
2.3 Electroweak contributions	6
2.4 Combination of electroweak and QCD corrections	8
3. Numerical results and discussion	9
3.1 Input parameters and event selection criteria	9
3.2 Monte Carlo tuning	12
3.3 Integrated cross sections (Tevatron and LHC)	13
3.4 PDF uncertainties (LHC)	16
3.5 Numerical results for the Tevatron	20
3.5.1 Observables for luminosity monitoring and PDF constraint	20
3.5.2 Observables for W precision physics	23
3.6 Numerical results for the LHC	26
3.6.1 Observables for luminosity monitoring and PDF constraint	27
3.6.2 Observables for W precision physics	29
3.6.3 Observables for new-physics searches	33
3.7 Results for jet multiplicity (Tevatron and LHC)	37
4. Conclusions and perspectives	38

1. Introduction

The electroweak gauge bosons W^\pm and Z^0 were discovered at the SpS collider at CERN more than twenty years ago [1]. Albeit a long time has passed since then, the production of electroweak gauge bosons in hadronic collisions is still a topic of deep interest in modern particle physics. Actually, single W and Z boson production is used at the Fermilab Tevatron collider to derive precision measurements of the W boson mass and width [2], to extract the electroweak (EW) mixing angle from the forward-backward asymmetry in the neutral current (NC) channel [3] and to severely constrain the Parton Distribution Functions (PDF) through the measurement of the W charge asymmetry [4]. These processes are also used for detector calibration and the measurement of their total production cross section can be compared with the corresponding QCD prediction, in order to test the convergence of the strong coupling expansion in perturbative QCD calculations [5, 6].

In the near future, at the Large Hadron Collider (LHC) at CERN, the production of W and Z bosons will continue to be a relevant process, because of its large cross section and very clean signature [7], given by one isolated charged lepton with missing transverse energy (for W production) and by two isolated charged leptons with opposite charges (for Z production). In particular, thanks to the very large statistics, a measurement of the W mass with an uncertainty of about 10 MeV should be feasible at the LHC [8, 9]. These processes are also good candidates to understand the detectors performances in the early stage of data analysis at the LHC [10], to monitor the collider luminosity with per cent precision [11, 12, 13] and constitute a background to new physics searches, noticeably new heavy gauge bosons Z' and W' [10, 14], whose discovery is an important goal of the LHC [5, 6].

It is important to realize that the many facets of the W/Z physics programme at hadron colliders require, for obvious reasons, the measurement of different observables, depending on the physics goal of interest. Correspondingly, a number of observables must be precisely predicted and simulated, to avoid theoretical bias in data analysis. For example, for precise W mass measurements the relevant observables are the W transverse mass and the lepton transverse momentum, while luminosity studies require a deep understanding of the total cross section, the W/Z rapidity and lepton pseudorapidity. On the other hand, the lepton pair invariant mass produced in Z production and the W transverse mass in their high tails are the observables to be focused on for the search for new physics signals.

To fully exploit the potential of the Tevatron and the LHC for all the above physics goals, the theoretical predictions have to be of the highest standard as possible. In particular, the high luminosity at the LHC implies that systematic errors, including theoretical ones, will play a dominant role in determining the accuracy of the cross sections. This requires to make available calculations of W and Z production cross sections including higher-order corrections originating from the EW and QCD sector of the Standard Model (SM). Furthermore, the implementation of such calculations in Monte Carlo (MC) generators is mandatory, in order to perform realistic studies of the impact of higher-order corrections on the observables and to compare theory with data.

In this paper we study the impact of electroweak and strong corrections, as well as of their combination, to the production process $p\bar{p}^{(-)} \rightarrow W \rightarrow \text{lepton} + X$. We also include in our analysis photon-induced contributions to $W \rightarrow \text{lepton} + X$ production and we provide results for top -pair production process, which may give rise to the signature of a high-transverse momentum lepton in association with missing energy, in order to include a non-negligible contribution for a precise evaluation of the overall background to new-physics searches. A similar study, which some of us have coauthored, has been recently performed for the NC Drell-Yan (DY) channel in the high invariant mass tail in [15], while an evaluation of the theoretical uncertainties in the cross sections of the charged current (CC) and NC processes around the W/Z peaks has been addressed in [16, 17] by strictly following the procedure presented by our group in some conference proceedings [18]. However, it is important to notice that at a difference with respect to (w.r.t.) the works [16, 17], where the effects of EW and QCD corrections are separately studied, in the present paper the combination of such effects is analyzed in detail, by providing different theoretical

recipes and discussing the related uncertainties. Furthermore, we provide also predictions for the transverse mass region above 1 TeV, which is an important range for new physics searches.

As far as complete $\mathcal{O}(\alpha)$ SM EW corrections to $pp^{(-)} \rightarrow W \rightarrow l\nu_l$ are concerned, they have been computed independently by various authors in [19, 20, 21, 22, 23, 24, 25]. Also one-loop corrections in the Minimal Supersymmetric Standard Model have been calculated in [26]. The predictions of a subset of such calculations have been compared, with the same input parameters and cuts, in [27, 28], finding a very satisfactory agreement. The contributions due to the emission of multiple photon radiation for the observables of interest for W precision physics have been calculated in [29, 30, 31, 32, 33, 26]. Comparisons of such multi-photon calculations can be found in [32, 33, 34], showing good agreement.

Concerning QCD calculations and tools, the present situation reveals quite a rich structure, that includes NLO/NNLO corrections to W total production rate [35, 36], fully differential cross sections known at NLO/NNLO QCD [37, 38, 39, 40, 41, 42], resummation of leading/next-to-leading logarithms arising from soft gluon radiation [43, 44], NLO corrections merged with parton shower evolution [45, 46, 47], as well as leading-order matrix elements generators matched with vetoed parton shower [48, 49, 50, 51].

A review of the theory of W and Z boson production can be found in [52, 53], while recent developments about QCD and generators are described in [54, 55].

On the other hand, it must be noticed that the combination of EW and QCD corrections is still at a very preliminary stage, only a few attempts being known in the literature [56, 57]. In particular, in [56] the effects of QCD resummation are combined with the leading part (in the statistically dominant region of the process around the W mass peak) of EW corrections, given by NLO final-state QED radiation and improved Born approximation to account for the pure weak corrections. Therefore, in the latter analysis the effect of purely (Sudakov-like) EW logarithms is missing, when it is known that the full set of EW corrections is required in addition to photonic corrections to reach a per cent theoretical precision [21, 22, 25]. Furthermore, in [54] the treatment of QCD effects is limited to the inclusion of multiple soft-gluon corrections, leaving room to more detailed studies of the QCD sources of contributions. The present situation of EW calculations and the recent development of more sophisticated QCD generators makes feasible a more complete analysis, both for what concerns QCD and EW effects.

Therefore, the aims of the present paper are the following:

1. to investigate the various sources of QCD effects (PDF uncertainties, comparison of presently available perturbative QCD calculations, allowing for variations of the factorization/renormalization scale), extending the analyses of [40, 56, 58] to consider the full set of observables of experimental interest and to make use of computational tools which include recent advances in QCD phenomenology;
2. to combine the results of the state-of-the-art of EW calculations with the QCD calculations and generators, that are typically used at the Tevatron and the LHC, in order to investigate the role of EW effects in association with QCD contributions;

3. to assess the reliability of existing tools and demonstrate the need of a deep understanding of QCD and of EW-QCD combination for precision physics studies at hadron colliders.

The outline of the paper is as follows. In Section 2 we review the main features of the theoretical tools used in our study, describing the treatment of PDF uncertainties (Section 2.1), the implementation of QCD effects according to different degrees of approximation in existing generators (Section 2.2), the treatment of NLO EW corrections and photon-induced processes (Section 2.3), as well as the combination of EW effects with strong corrections (Section 2.4), which is the main theoretical feature of the paper. In Section 3 we present and discuss the numerical results for the observables that are grouped on the basis of their specific experimental motivation, both at the energies of the Fermilab Tevatron proton-antiproton ($p\bar{p}$) collider and of the CERN LHC proton-proton (pp) collider. Conclusions and possible developments of our work are drawn in Section 4.

2. Theoretical ingredients

2.1 Parton Distribution Functions (PDF)

It is widely documented [59] that a precise knowledge of the partonic structure of the proton will be an essential ingredient for the physics potentials of the LHC, both for what concerns discovery and precision physics. At present, there is a great deal of interest in understanding how the uncertainties on the determination of the Parton Distribution Functions (PDF), both of experimental and theoretical origin, translate into uncertainties for those observables that will be measured at the LHC. A short review of recent progress in Parton Distributions and implications for LHC physics can be found in [60]. A parton distribution library, known as LHAPDF [61], is available and gives the possibility of comparing different PDF parameterizations.

In particular, some sets allow to estimate how the errors of the experimental measurements affect the PDF parameterization within a certain practical tolerance. The latter is defined as the maximum allowed of the $\Delta\chi^2$ variation w.r.t. the parameters of the best PDF fit. In our analysis, among the PDFs sets available in LHAPDF, we will make use of MRST2001E [62] and CTEQ6 [63], as done in previous similar studies [58, 64]. For these two different sets of NLO PDFs the tolerance T is assumed to be $T = \sqrt{50}$ (MRST2001E) and $T = 10$ (CTEQ6), resulting in PDFs uncertainties larger for a factor of $\sqrt{2}$ for CTEQ6. It is worth emphasizing that the uncertainties obtained according to such a procedure are purely experimental (i.e. as due to the systematic and statistical errors of the data used in the global fit), leaving aside other sources of uncertainty of theoretical origin, such as, for example, uncertainties due to the truncation of DGLAP perturbation expansion, choice of the parameterization of non-perturbative input PDF or $\ln(1/x)$ effects. However, they can be estimated separately and it is known from previous studies [65, 66] that the theory-induced uncertainty is similar in magnitude to the uncertainty due to experimental errors at the Tevatron, but larger at the LHC. However, in analogy to previous phenomenological studies [58, 64], we limit to consider PDFs uncertainties deriving from errors on the data,

just to get an idea of the order of magnitude of such effects in comparison with the size of perturbative corrections that are the main subject of our analysis.

Finally, we point out that, since we include in our predictions EW corrections and, therefore, we need to treat collinear singularities due to photon radiation off the initial state quarks for the sake of consistency at NLO EW, it is necessary a set of PDF including QED effects in DGLAP evolution. The MRST group performed a global PDFs analysis including QED contributions, which have been incorporated in the set of PDFs known as MRST2004QED [67]. It turns out that the QED evolution slightly modifies the standard QCD-evolved PDFs for typical x and Q^2 values probed by weak boson production at the Tevatron and the LHC, as already argued in previous studies [68, 69, 70]. However, it must be stressed that the inclusion of QED corrections into PDFs dynamically generates a photon density inside the (anti)proton. This implies that EW processes initiated by a photon (photon-induced processes) contribute to EW gauge boson production in hadronic collisions, as discussed in Section 2.3. As largely discussed in the literature, the present PDF uncertainties are expected to be significantly reduced when LHC data will become available.

The parameterizations MSTW [71] and CTEQ6.6 [72], appeared in the literature during the completion of the present work, will be discussed shortly in Section 3.4.

2.2 QCD corrections and Monte Carlo tools

The QCD codes typically used in high-energy collider experiments are “general purpose” parton shower MC’s, such as, for example, HERWIG [74] or PYTHIA [75], Apac++ [76] or MC programs based on a fixed-order perturbative calculation of a given process. However, the new challenges of the Tevatron Run II and the LHC have spurred on improved approaches to QCD MC’s and calculations, including the matching of exact leading-order matrix elements for multiparticle production with parton shower, the matching of NLO corrections with parton shower, advances in the techniques for NNLO calculations, as well as improvements in the parton shower algorithms [54, 55, 77, 78].

As already remarked in the Introduction, we make use in our analysis, for the sake of definiteness, of those QCD calculations and relative codes that are already used at the Tevatron or will be presumably used at the LHC for data analysis, and, at least in our opinion, are representative of those advances sketched above. We therefore consider the following set of programs

1. ALPGEN [48]: it is a code for the generation of many multiparton processes in hadronic collisions, computing exact matrix elements by means of the ALPHA algorithm [79]. The leading-order matrix elements are matched with appropriate Sudakov form factors to add parton shower effects (according to the so-called MLM prescription to match matrix elements and parton shower [80, 81, 82, 83, 84]) and by vetoing shower evolution leading to multiparton final states already described by the matrix element computation. A review of the matching algorithm implemented in ALPGEN and here used can be found in [84], while a comparison between the predictions of the

different procedures of matrix elements-parton shower matching is given in [85, 86]. Additional information is available at <http://mlm.home.cern.ch/mlm/alpgen/>

2. MCFM [37]: it is a program for the MC simulations of various processes at hadron colliders, giving predictions, for most processes (including W/Z production), at NLO in QCD and incorporating full spin correlations. It is available, together with a detailed documentation, at <http://mcfm.fnal.gov>
3. MC@NLO [45]: it is a generator incorporating NLO QCD corrections into the parton-shower generator HERWIG for a large class of processes. As such, MC@NLO provides a consistent description of exact $\mathcal{O}(\alpha_s)$ emission effects together with a leading-logarithmic resummation of soft and collinear QCD radiation. More details can be found at <http://www.hep.phy.cam.ac.uk/theory/webber/MCatNLO/>
4. ResBos [43, 44]: it is a MC integrator program, presently used at the Tevatron, that computes fully differential cross sections of various boson production processes in hadron-hadron collisions, including DY-like processes, either with NLO initial-state QCD corrections, or with soft-gluon initial-state resummed QCD corrections, the latter according to the Collins, Soper and Sterman (CSS) resummation formalism [87]. Recently, Resbos has been improved by the inclusion of final-state NLO electromagnetic contributions to W boson production [56], resulting in the ResBos-A code. More information can be found at <http://hep.pa.msu.edu/resum/>. Since in our study we are interested in both QCD and EW effects, we use, among the different ResBos versions available on the web, the ResBos-A generator, including CSS resummation and final-state QED radiation, making use of the grids publicly available for the Tevatron energy
5. FEWZ [40, 41]: it is a code computing fully differential cross sections at NLO/NNLO in perturbative QCD for W and Z boson production in hadron collisions, including finite-width effects and full spin correlations.
It is available at <http://www.phys.hawaii.edu/~kirill/FEHiP.htm>

As far as FEWZ is concerned, it will be used in the present paper for tuning purposes at the NLO level for fully integrated cross sections. Its predictions at the NNLO level and the phenomenological relevance of NNLO corrections have already been analyzed in [16, 17].

It should also be mentioned that a recent advance in the QCD predictions for DY processes is represented by the calculation of [46]. This consistently combines the NLO QCD corrections with parton shower resummation, avoiding negative weights in the generation of events, and is available in the MC POWHEG. We will not show in our analysis predictions of POWHEG, since they are already compared with MC@NLO [47], finding fair agreement for *jet*-inclusive quantities.

2.3 Electroweak contributions

The radiative corrections originating from the EW sector of the SM are taken into account in our analysis according to the recent calculation of [25], which the reader is ad-

dressed to for more details. At a variance of QCD corrections, we do not need to take into consideration here the results of different, independent calculations because it is known from recent tuned-comparison studies [27, 28] that the predictions of those calculations typically used or under consideration by hadron collider collaborations, such as DK [21], SANC [24] and WGRAD [20, 22], are in very good agreement with the results of HORACE, which is the generator implementing the theoretical formulation of [25], available at <http://www.pv.infn.it/~hepcomplex/horace.html>. In HORACE, the exact one-loop EW corrections to the CC DY process are consistently matched with higher-order leading logarithms due to multiple photon emission, that have been shown to be not irrelevant for the precision target of W mass measurements at hadron colliders [29, 30]. By itself, HORACE does not include any effect due initial-state QCD parton shower, but the events generated with it can be interfaced with standard shower MC programs.

Since we are interested in a detailed description of EW effects too, we need to include in our calculation, for the sake of consistency, also the contribution of the so-called photon-induced processes $\gamma q \rightarrow q' l \nu_l$ and $\gamma \bar{q}' \rightarrow \bar{q} l \nu_l$ (see Figure 1). Actually, these processes are of the same EW perturbative order of one-loop EW corrections and give rise to the same signature of the inclusive W production process. Furthermore, their contribution has been

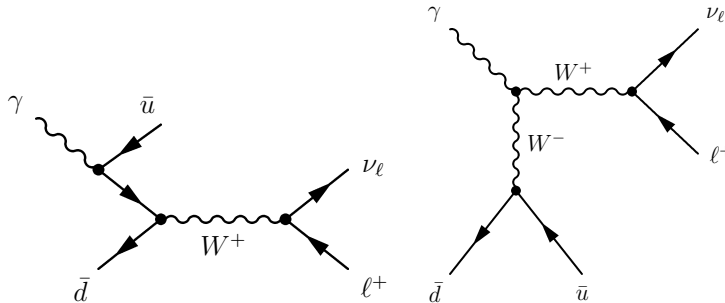


Figure 1: Examples of Feynman diagrams for the photon-induced processes

shown by Dittmaier-Krämer in [27] to be non negligible for W -boson production in the presence of realistic event selection cuts at the LHC. The matrix elements for the photon-induced processes ($\gamma q \rightarrow q' l \nu_l$) are obtained by crossing symmetry from the $q \bar{q}' \rightarrow l \nu_l \gamma$ matrix elements, already available from the calculation of hard-bremsstrahlung diagrams contributing to EW corrections.

It is worth noting that the inclusion of photon-induced processes introduces in the $\mathcal{O}(\alpha)$ -corrected parton-level cross section mass singularities due to a collinear splitting $\gamma \rightarrow q \bar{q}$. As for photon radiation off the initial-state quarks present in the NLO EW calculation and, again, in analogy with factorization in NLO QCD calculations, the collinear singularities due to $\gamma \rightarrow q \bar{q}$ collinear splitting can be absorbed in the distribution functions, by replacing the (anti-)quark distribution as described in detail, with all the necessary formulae, in [88].

2.4 Combination of electroweak and QCD corrections

The aim of this Section is to describe how the contributions of EW origin are combined, in our approach, with QCD predictions.

A first strategy for the combination of EW and QCD corrections consists in the following additive formula

$$\left[\frac{d\sigma}{d\mathcal{O}} \right]_{\text{QCD\&EW}} = \left\{ \frac{d\sigma}{d\mathcal{O}} \right\}_{\text{QCD}} + \left\{ \left[\frac{d\sigma}{d\mathcal{O}} \right]_{\text{EW}} - \left[\frac{d\sigma}{d\mathcal{O}} \right]_{\text{LO}} \right\}_{\text{HERWIG PS}} \quad (2.1)$$

where $d\sigma/d\mathcal{O}_{\text{QCD}}$ stands for the prediction of the observable $d\sigma/d\mathcal{O}$ as obtained by means of one of the QCD generators described in Section 2.2, $d\sigma/d\mathcal{O}_{\text{EW}}$ is the HORACE prediction for the EW corrected $d\sigma/d\mathcal{O}$ observable, and $d\sigma/d\mathcal{O}_{\text{LO}}$ is the lowest-order hadron-level result. The label HERWIG PS in the second term in r.h.s. of eq. (2.1) means that EW corrections are convoluted with QCD PS evolution through the HERWIG event generator, in order to (approximately) include mixed $\mathcal{O}(\alpha\alpha_s)$ corrections and to obtain a more realistic description of the observables under study. In principle, concerning QCD, the predictions of any of the codes considered in Section 2.2 could be used in eq. (2.1). However, because in our approach EW corrections are treated at NLO and are convoluted with the QCD parton shower cascade by HERWIG, it follows that, in eq. (2.1), the QCD contributions can be consistently combined with EW effects only by making use of the results provided, among the different QCD generators, by MC@NLO, in order to treat QCD NLO and shower corrections on the same ground of the EW counterpart. Therefore, in the following, we will show results for the QCD and EW combination assuming $[d\sigma/d\mathcal{O}]_{\text{QCD}} \equiv [d\sigma/d\mathcal{O}]_{\text{MC@NLO}}$ ¹. This implies, in turn, that the HORACE and MC@NLO generators need to be properly tuned at the level of input parameters and PDF set, in order to provide meaningful predictions. Furthermore, since we are interested in consistent comparisons between the results of independent codes, this tuning procedure has to be applied to each generator in use, as discussed in Section 3.2. Concerning the convolution of NLO EW corrections with QCD PS, it is worth noting that, according to eq. (2.1), the contributions of the order of $\alpha\alpha_s$ are not reliable when hard non-collinear QCD radiation turns out to be relevant, e.g. for the lepton and vector boson transverse momentum distributions in the absence of severe cuts able to exclude resonant W production. In this case, a full $\mathcal{O}(\alpha\alpha_s)$ calculation would be needed for a sound evaluation of mixed EW and QCD corrections. Full $\mathcal{O}(\alpha)$ EW corrections to the exclusive process $pp \rightarrow W + j$ (where j stands for jet) have been recently computed, in the approximation of real W bosons, in [89, 90], and for off-shell W in [91], while one-loop weak corrections to Z hadro-production have been computed, for on-shell Z bosons, in [92]. It is also worth stressing that in eq. (2.1) the infrared part of QCD corrections is factorized, whereas the infrared-safe matrix element residue is included in an additive form.

¹Alternatively one could use POWHEG in association with PYTHIA PS, without spoiling the general procedure presented here.

It is otherwise possible to implement a fully factorized combination as follows:

$$\left[\frac{d\sigma}{d\mathcal{O}} \right]_{\text{QCD} \otimes \text{EW}} = \left(1 + \frac{[d\sigma/d\mathcal{O}]_{\text{MC@NLO}} - [d\sigma/d\mathcal{O}]_{\text{HERWIG PS}}}{[d\sigma/d\mathcal{O}]_{\text{LO/NLO}}} \right) \times \left\{ \frac{d\sigma}{d\mathcal{O}_{\text{EW}}} \right\}_{\text{HERWIG PS}}, \quad (2.2)$$

where the ingredients are the same as in eq. (2.1) but also the QCD matrix element residue is now factorized. It is worth noticing that the QCD correction factor in front of $\{d\sigma/d\mathcal{O}_{\text{EW}}\}_{\text{HERWIG PS}}$ is defined in terms of two different normalization cross sections, namely the LO or the NLO one, respectively. As it can be easily checked, the two prescriptions differ at the order α_s^2 by non-leading contributions. Nevertheless, eq. (2.2) normalized in terms of the LO cross section can give rise to pathologically large order α_s^2 corrections in the presence of huge NLO effects, as will be discussed in the next section. On the other hand, when NLO matrix element effects do not introduce particularly relevant corrections, the two prescriptions are substantially equivalent, as it will be demonstrated too in the discussion of numerical results. Some comments are in order here. Equations (2.1) and (2.2) in both prescriptions have the very same $\mathcal{O}(\alpha)$ and $\mathcal{O}(\alpha_s)$ content. While the two factorized prescriptions contain the same $\mathcal{O}(\alpha\alpha_s)$ contributions, the additive prescription has mixed $\mathcal{O}(\alpha\alpha_s)$ contributions which differ from the factorized recipes. Therefore, their relative difference can be taken as an estimate of the uncertainty of QCD and EW combination and will be discussed in detail in the next section.

3. Numerical results and discussion

3.1 Input parameters and event selection criteria

The numerical results have been obtained using *in each code* the following values for the input parameters

$G_\mu = 1.16639 \cdot 10^{-5} \text{ GeV}^{-2}$	$m_W = 80.419 \text{ GeV}$	$m_Z = 91.188 \text{ GeV}$
$\Gamma_W = 2.048 \text{ GeV}$	$\sin^2 \theta_W = 1 - m_W^2/m_Z^2$	$m_H = 120 \text{ GeV}$
$m_e = 510.99892 \text{ KeV}$	$m_\mu = 105.658369 \text{ MeV}$	$m_\tau = 1.77699 \text{ GeV}$
$m_u = 320 \text{ MeV}$	$m_c = 1.55 \text{ GeV}$	$m_t = 174.3 \text{ GeV}$
$m_d = 320 \text{ MeV}$	$m_s = 500 \text{ MeV}$	$m_b = 4.7 \text{ GeV}$
$V_{cd} = 0.224$	$V_{cs} = 0.975$	$V_{cb} = 0$
$V_{ud} = \sqrt{1 - V_{cd}^2}$	$V_{us} = 0.224$	$V_{ub} = 0$
$V_{td} = 0$	$V_{ts} = 0$	$V_{tb} = 1$

and adopting the G_μ input scheme for the calculation of EW corrections, where, in particular, the effective electromagnetic coupling constant is given in the tree-level approximation by

$$\alpha_{G_\mu}^{\text{tree}} = \frac{\sqrt{2} G_\mu \sin^2 \theta_W m_W^2}{\pi} \quad (3.1)$$

However, for the coupling of external photons to charged particles needed for the evaluation of photonic corrections we use $\alpha(0) = 1/137.03599911$.

We study the production process $p\bar{p} \rightarrow \text{lepton} + X$, both at the Tevatron $p\bar{p}$ collider ($\sqrt{s} = 1.96$ TeV) and at the pp LHC ($\sqrt{s} = 14$ TeV), presenting results only for final-state muons, for the sake of definiteness. Actually, the difference between electron and muon final states is confined at the level of pure EW and multiple photon corrections, and can be inferred from the literature addressing such a topic in detail [20, 21, 25, 29, 30].

Tevatron	
$p_{\perp}^l \geq 25$ GeV	$\cancel{E}_T \geq 25$ GeV and $ \eta_l < 1.2$
$p_{\perp}^W \leq 50$ GeV	$50 \text{ GeV} \leq M_{l\nu} \leq 200$ GeV

Table 1: Selection criteria for the Tevatron

LHC	
a. $p_{\perp}^l \geq 25$ GeV	$\cancel{E}_T \geq 25$ GeV and $ \eta_l < 2.5$
b. the cuts as above	$\oplus \quad M_{\perp}^W \geq 1$ TeV

Table 2: Selection criteria for the LHC

The selection criteria used for our analysis at the Tevatron and the LHC are summarized in Table 1 and Table 2, respectively. In the Tables p_{\perp}^l and η_l are the transverse momentum and the pseudorapidity of the muon, \cancel{E}_T is the missing transverse energy, which we identify with the transverse momentum of the neutrino, as typically done in phenomenological studies [20, 21, 22, 25, 56, 58]; p_{\perp}^W and M_{\perp}^W are the transverse momentum and transverse mass of the W boson, $M_{l\nu}$ is the invariant mass of the muon-neutrino pair. The selection criteria in the first line of Table 1 are introduced to model the acceptance cuts used by the experimental collaborations at the Tevatron, while the constraints on p_{\perp}^W and $M_{l\nu}$ in the second line are imposed in order to include in our study of the QCD corrections the predictions of ResBos-A v1.1, which makes publicly available grids for numerical integration corresponding to such constraints. For the LHC, we consider two different set up, labeled as a. and b. in Table 2. The first one corresponds to typical cuts used for LHC simulations, while for the second one a severe cut on the W transverse mass is superimposed to the cuts of set up a., in order to isolate the region of the high tail of M_T^W , which is interesting for new physics searches.

In order to avoid edge effects in the final phenomenological analysis, introduced by cuts at the generation level, we make use of the following loose generation cuts $p_{\perp}^l \geq 5$ GeV, $\cancel{E}_T \geq 5$ GeV, $|\eta_l| < 5$ (for both the Tevatron and set up a. at the LHC), with, additionally, $M_{\perp}^W \geq 0.8$ TeV for set up b. at the LHC. These cuts have been imposed simply to improve the efficiency in the generation of MC events. For the ALPGEN code, we also use the following generation cuts for additional QCD partons: $p_T > 20$ GeV, $|\eta_j| < 5$, $\Delta R_{ij} > 0.7$, where ΔR_{ij} is the separation between the i -th and j -th parton in the $\eta - \phi$ plane. The parameters required in ALPGEN for the matching between matrix elements and shower

evolution are chosen as: $E_{T,clus.} = 25$ GeV, $|\eta_j| = 5$, $R_j = 1.05$, as done in previous studies [84, 85, 86]. A first attempt to assess the intrinsic systematics associated with the matching procedure has been presented in [86]. For our purposes we assume that the up to one jet samples are well described by NLO and next-next leading logarithmic codes. Therefore the impact of the uncertainties of the matching procedure is related to the importance of higher parton multiplicities for the various distributions under consideration. As it will be shown in the following, their size is at the level of (or below) 1% at the Tevatron and the LHC (event selection a), while they become more relevant at the LHC, event selection b), where a more thorough investigation could be worthwhile.

The set of parton density functions used in our study is CT6EQ6M [63] for the case of the Tevatron, with factorization/renormalization scale $\mu_R = \mu_F = M_{l\nu}$ for both the LO and NLO predictions. Again, this choice has been dictated by the necessity of including ResBos-A in our comparisons. Although it is theoretically inconsistent using a PDF set, like CT6EQ6M, without QED contributions when combining QCD corrections with NLO EW contributions, it is also known, as previously discussed, that the effect of QED evolution is small and translates into negligible numerical effects on the observables of interest here within the adopted selection criteria.

For the LHC, all the analysis is performed using the set MRST2004QED, in order to consistently incorporate EW corrections and photon-induced processes in association with QCD corrections. For the LHC, the QCD factorization/renormalization scale and the analogous QED scale (present in MRST2004QED) are chosen to be equal, as usually done in the literature [20, 21, 22, 25], and fixed at $\mu_R = \mu_F = \sqrt{p_{\perp W}^2 + M_{l\nu}^2}$, where $M_{l\nu}$, as done in previous studies [58], both for LO and NLO results.

The numerical results showing the estimate of the PDF uncertainties on the observables at the LHC energies (Section 3.4) have been obtained using the generator MC@NLO version 3.3 implementing the LHAPDF package. Results for the NLO MRST2001E (with 30 error sets) and CTEQ6 (with 40 error sets) parameterizations as available in LHAPDF are shown, using as default scale choice $\mu_R = \mu_F = \sqrt{p_{\perp W}^2 + M_{l\nu}^2}$.

For $\alpha_s(Q^2)$ we use as input parameters $\alpha_s(M_Z) = 0.118$ at the Tevatron and $\alpha_s(M_Z) = 0.121$ at the LHC. We checked that for all the codes under consideration the values of α_s agree at the 0.1% level when varying Q from M_Z to a few TeV.

All the numerical simulations have been done without taking into account the effects of the underlying event and hadronization processes.

The numerical results discussed in the following have been obtained according to a MC statistics of approximately 10^6 - 10^8 events for the integrated sections and of about 10^6 events for the distributions. For the integrated cross sections, the numbers in the Tables quoted in parenthesis after the last digit correspond to the 1σ MC errors. As for the distributions, each of them has been generated as an histogram consisting of 25 bins. Therefore, in the dominant region of a given distribution (e.g. in the central range of the W rapidity and lepton pseudorapidity and around the Jacobian peak of the W transverse mass and lepton transverse momentum), the statistical uncertainty associated to the cross section in a bin is at the level of some per mille. In the tails of the distributions, the MC

error can grow up to a few per cent level. This statistics is sufficient for a meaningful interpretation of the effects of interest in the present study and discussed in the following. Actually, whenever rather mild effects are registered (e.g. of a few per cent), they typically show up in the dominant regions where the statistical uncertainty is about a factor of ten smaller. On the other hand, in the tails of the distributions, characterized by a poorer statistics, the contributions of interest are typically quite large (at the level of several or tens of per cent) and are therefore meaningful in comparison with the size of the statistical fluctuations. Last but not least, the most moderate effects generally correspond, as it will be shown in the following, to the difference between the results of the additive and factorized recipes for the combination of EW and QCD corrections. However, since the two recipes are defined in terms of the very same theoretical ingredients, and use the same MC data, it turns out that predictions of the two combinations are strongly correlated variables and, as such, the uncertainty associated to each of these two predictions largely cancel out when considering the difference of the two.

3.2 Monte Carlo tuning

Before discussing the numerical results, we would like to spend some words about the effort done in MC tuning, in order to normalize all the codes to the same LO or NLO cross section and, therefore, avoid possible bias in the interpretation of the physical effects of interest.

Concerning the program ResBos-A, we switched off some EW contributions present inside the code in the form of Improved Born Approximation and transformed the running W width in the W propagator into a fixed width, to normalize the code at a pure LO cross section. Moreover, we used the program without NLO QED final-state corrections when providing pure QCD predictions.

To tune FEWZ against the other codes, we substituted the default choice of using the experimental branching ratio $\text{BR}(W \rightarrow \mu\nu)$ with the tree-level theoretical branching ratio $\Gamma(W \rightarrow \mu\nu)/\Gamma(W \rightarrow \text{all}) = 1/9$, for consistency with the other used programs.

As far as MC@NLO is concerned, we tuned it at the next-to-leading-order in QCD, by comparing its predictions with the corresponding NLO QCD results of FEWZ and MCFM. This tuning has been performed at the level of completely inclusive (i.e. without cuts) cross sections both for the Tevatron and the LHC, as well as in the presence of a cut on the invariant mass $M_{l\nu} > 0.8$ TeV at LHC energies, in order to check the correct normalization in the region important for new-physics studies.

Monte Carlo	ALPGEN	FEWZ	HORACE	MCFM	ResBos-A
σ_{LO} (pb)	906.3(3)	905.4(2)	905.6(1)	905.1(1)	905.3(2)

Table 3: MC tuning at the Tevatron for the LO cross sections of the sum of the processes $p\bar{p} \rightarrow W^+ \rightarrow \mu^+ + \nu$ and $p\bar{p} \rightarrow W^- \rightarrow \mu^- + \bar{\nu}$, according to the cuts of Table 1 and using the CT6EQ6M PDFs with scale $M_{l\nu}$.

The results are shown in Table 3 for the LO cross sections at the Tevatron, in Table 4 for the LO cross sections at the LHC, in Table 5 for the tuning between FEWZ, MCFM

Monte Carlo	ALPGEN	FEWZ	HORACE	MCFM
σ_{LO} (pb)	8310(2)	8306(1)	8308(1)	8305(1)

Table 4: MC tuning at the LHC for the LO cross sections of the sum of the processes $pp \rightarrow W^+ \rightarrow \mu^+ + \nu$ and $pp \rightarrow W^- \rightarrow \mu^- + \bar{\nu}$, according to the cuts of set up a. in Table 2 and using the MRST2004QED PDFs with scale $\sqrt{p_{\perp W}^2 + M_{l\nu}^2}$

Monte Carlo	FEWZ	MC@NLO	MCFM
$\sigma_{\text{NLO}}^{\text{Tevatron}}$ (pb)	2635.5(4)	2639.1(5)	2640(1)
$\sigma_{\text{NLO}}^{\text{LHC}}$ (pb)	21058(3)	21031(3)	21008(2)

Table 5: MC tuning at the Tevatron and LHC for MC@NLO and MCFM NLO inclusive cross sections of the sum of the processes $pp^{(\pm)} \rightarrow W^- \rightarrow \mu^- \bar{\nu}$ and $pp^{(\pm)} \rightarrow W^+ \rightarrow \mu^+ \bar{\nu}$, using the PDF sets CT6EQ6M at the Tevatron with scale $M_{l\nu}$ and MRST2004QED at the LHC with scale $\sqrt{p_{\perp W}^2 + M_{l\nu}^2}$, respectively.

Monte Carlo	MC@NLO	MCFM
σ_{NLO} (fb)	50.34(1)	50.28(2)

Table 6: MC tuning at the LHC for MC@NLO and MCFM NLO cross sections of the sum of the processes $pp \rightarrow W^- \rightarrow \mu^- \bar{\nu}$ and $pp \rightarrow W^+ \rightarrow \mu^+ \bar{\nu}$, in the presence of a cut on the invariant mass $M_{l\nu} > 0.8$ TeV and no other lepton selection criteria. The PDF set is MRST2004QED with scale $\sqrt{p_{\perp W}^2 + M_{l\nu}^2}$.

and MC@NLO NLO inclusive cross section both at the Tevatron and LHC, and in Table 6 for the MCFM and MC@NLO predictions at LHC energies when imposing the invariant mass cut $M_{l\nu} > 0.8$ TeV. As can be seen, there is a very good agreement between the predictions of the different programs, since all the relative differences are at the few per mille level (or better), i.e. much smaller than the size of the radiative corrections discussed in the following. As already remarked in [15], the tuning procedure is essential because it validates the interpretation of the various contributions as due to physical effects and not to a mismatch in the set up of the codes under consideration.

3.3 Integrated cross sections (Tevatron and LHC)

In Table 7 and Table 8 we present the results for the integrated cross sections corresponding to the selection criteria at the Tevatron and LHC quoted in Section 3.1, as obtained according to the following codes and theoretical recipes

1. Leading order, as obtained by MCFM code in terms of the LO matrix element supplemented by the PDF sets defined in Section 3.1
2. ALPGEN S_0 : the hadron-level LO cross section of the CC DY process is convoluted with parton shower evolution through HERWIG Parton Shower. Hence, such a prediction can be considered as analogous to that of a pure parton shower generator;

3. ALPGEN S_1 : the exact LO matrix elements for up to one parton radiation are interfaced to HERWIG parton shower, according to the MLM prescription of matrix elements-PS matching;
4. ALPGEN S_2 : the exact LO matrix elements for up to two parton radiation are interfaced to HERWIG parton shower, according to the MLM prescription of matrix elements-PS matching;
5. MCFM, i.e. pure NLO QCD predictions (MCFM NLO QCD), including also factorization and renormalization scale variation by varying them by a factor 1/2 or 2 around the central values specified in Section 3.1 (see Table 8);
6. HORACE NLO EW: HORACE, in the presence of NLO EW corrections;
7. HORACE NLO+HERWIG PS: the NLO EW predictions of HORACE are interfaced with HERWIG QCD Shower evolution;
8. MC@NLO: NLO QCD combined with HERWIG parton shower;
9. ResBos-A CSS: ResBos-A, with pure QCD CSS resummation, without fixed-order perturbative QCD contributions and final-state QED radiation;
10. ResBos-A NLO QED: without QCD resummation, without fixed-order perturbative QCD results but with final-state QED radiation;
11. ResBos-A, as far as its complete predictions, including QCD resummation and final-state QED radiation, but without perturbative QCD corrections, are concerned;
12. Equation (2.1), obtained by summing the predictions of MC@NLO with those of HORACE NLO convoluted with HERWIG PS according to eq. (2.1) (additive combination);
13. Equation (2.2), for the combination of QCD and EW contributions in factorized form.

As can be seen from Table 7 and, in particular from the comparison between the LO results and the ALPGEN S_0 predictions, the QCD PS effects lower the cross section by about $10 \div 15\%$ at the Tevatron and LHC set up a, while they are negligible at LHC set up b. The exact matrix element corrections, as present in ALPGEN S_2 , are not relevant for the cross section at the Tevatron, while they induce a some per cent (positive) contribution for the two set up at the LHC.² The NLO QCD corrections are positive, of about 8%, at the Tevatron, negative of about 2% at the LHC set up a and positive of about 20% at the LHC set up b. The EW corrections are at the level of a few per cent and negative at the Tevatron and LHC set up a., while they are quite large, of the order of -25% , for set up b. at the LHC, in agreement with the results of various studies in the literature on the virtual EW Sudakov logarithms. It is worth noticing that for the considered event

²The results of ALPGEN S_1 are not shown in Table 7 because they are practically indistinguishable, within the statistical errors of the MC integration, from the predictions of ALPGEN S_2 .

	Tevatron	LHC	
Prediction		a.	b.
Leading order	905.1(1)	8305(1)	7.128(3)
ALPGEN S_0	815(1)	7224(5)	7.15(1)
ALPGEN S_2	814(1)	7578(5)	7.29(1)
MCFM NLO QCD	979.1(6)	8135(2)	8.681(2)
HORACE NLO EW	881.5(2)	8091(1)	5.569(2)
HORACE NLO+HERWIG PS	792(1)	7008(5)	5.55(1)
MC@NLO	967(3)	8254(5)	8.64(1)
ResBos-A CSS	933.4(4)	–	–
ResBos-A NLO QED	877.9(3)	–	–
ResBos-A	920(3)	–	–
Eq. (2.1) QCD+EW add.	944(3)	8038(9)	7.04(2)
Eq. (2.2) QCD \otimes EW fact. LO	925(3)	7877(8)	6.71(2)
Eq. (2.2) QCD \otimes EW fact. NLO	915(3)	7895(8)	6.50(1)

Table 7: Integrated cross sections, relative to the selection criteria of Table 1 and Table 2, according to different approximations for the various programs considered in the study. For the Tevatron and set up a. at the LHC the cross sections are given in pb, while the units of measure are fb for set up b. at the LHC.

selection the NLO QCD and EW corrections tend to compensate at the Tevatron and LHC set up b, while they sum up coherently at the LHC set up a. The QCD PS, when convoluted with the NLO EW contributions, decreases the cross sections of about 10%, as already noted above at the level of pure QCD results, at the Tevatron and the LHC set up a, while it is irrelevant at the LHC set up b. The combination of NLO QCD corrections with PS resummation, as predicted by MC@NLO, gives a correction at the per cent level w.r.t. the pure NLO QCD correction obtained with MCFM. The soft-gluon resummation a la CSS is responsible of a few per cent increase of the LO cross section at the Tevatron, while NLO final-state QED radiation is of the same order but of opposite sign, so that the two effects tend to compensate, yielding a full ResBos-A prediction of only about 1% larger than the LO cross section. On the other hand, the combination of EW and QCD corrections according to the (additive) formula of eq. (2.1) predicts an enhancement of the LO cross section at the Tevatron of about 7%, differing of some per cent from the ResBos-A result, as a consequence of the different QCD and EW ingredients between eq. (2.1) and the ResBos-A formulation. The calculation of the combined EW and QCD as in the (factorized) formula of eq. (2.2) differs from the additive prediction of about 2%, thus reducing the difference w.r.t. ResBos-A. At the LHC, the combined QCD/EW correction is negative, of the order of few per cent, both in the set up a and b. It is worth noticing, however, that in the set up a this is due to the sum of mild corrections of the same sign, whereas in the set up b it is the result of the almost complete cancellation of large QCD and EW corrections. Also in this case, the difference of additive and factorized prescriptions

amounts to few per cent.

Collider	$\sigma_{\text{NLO}}^{(\mu/2)}$	$\sigma_{\text{NLO}}^{(\mu)}$	$\sigma_{\text{NLO}}^{(2\mu)}$
Tevatron	978.5(8)	979.1(6)	987.1(6)
LHC a.	7875(1)	8135(2)	8393(2)
LHC b.	8.890(5)	8.681(2)	8.501(4)

Table 8: NLO cross sections, including scale variation, as obtained by means of MCFM at the Tevatron and LHC, set up a. and b. The cross sections are given in pb for the Tevatron and set up a. at the LHC, in fb for set up b. at the LHC.

In Table 8 we show the NLO predictions of MCFM at three different factorization/re-normalization scales, $\mu_R = \mu_F = \mu/2, \mu, 2\mu$, as it is customary, with $\mu = M_{l\nu}$ at the Tevatron and $\mu = \sqrt{p_{\perp W}^2 + M_{l\nu}^2}$ at the LHC. The scale dependence at the Tevatron is at the 1% level, indicating a good stability of the NLO prediction for the assumed scales. At the LHC set up a., the cross section varies of about 3-4% as a function of the scale variation, while a 2% variation is observed for the cross section at the LHC set up b. As a whole, the results shown in Table 7 point out the following aspects: first of all, a proper combination of EW and QCD corrections is mandatory to achieve a cross section accuracy of the order of a few per cent, in particular for the set up b at the LHC where a subtle cancellation occurs; secondly, at the per cent accuracy the NNLO QCD corrections should be taken into account, being their contribution of a few per cent as estimated by the scale variations shown in Table 8 and confirmed by dedicated calculations in the literature [40, 41, 16, 17, 42]; last, at such a precision level also exact mixed $\mathcal{O}(\alpha\alpha_s)$ contributions, at present not known, can be expected to be relevant as pointed out by the relative difference between the additive and factorized prescriptions of eqs. (2.1) and (2.2), respectively.

3.4 PDF uncertainties (LHC)

In this Section we discuss how the PDFs uncertainties of experimental origin, as known of today, affect all the observables of interest for the physics analysis of the process $pp \rightarrow \mu + X$ at the LHC.

In Figure 2 we show the results for the W rapidity and muon pseudorapidity (upper plots) and for the W transverse mass and muon transverse momentum (lower plots) according to set up a. specified in Table 2, as obtained with the NLO CTEQ61 parameterization available in the LHAPDF package.

For each observable, we show the predictions corresponding to the maximum and minimum values returned by CTEQ61 PDFs, together with the result of the best fit parton densities.

The PDF uncertainty for an observable O is the maximal change in O as a function of variables $\{z_i\}$ varying within the tolerance hypersphere [93]:

$$\delta O = \sqrt{\sum_{i=1}^{n/2} \delta O_i^2}$$

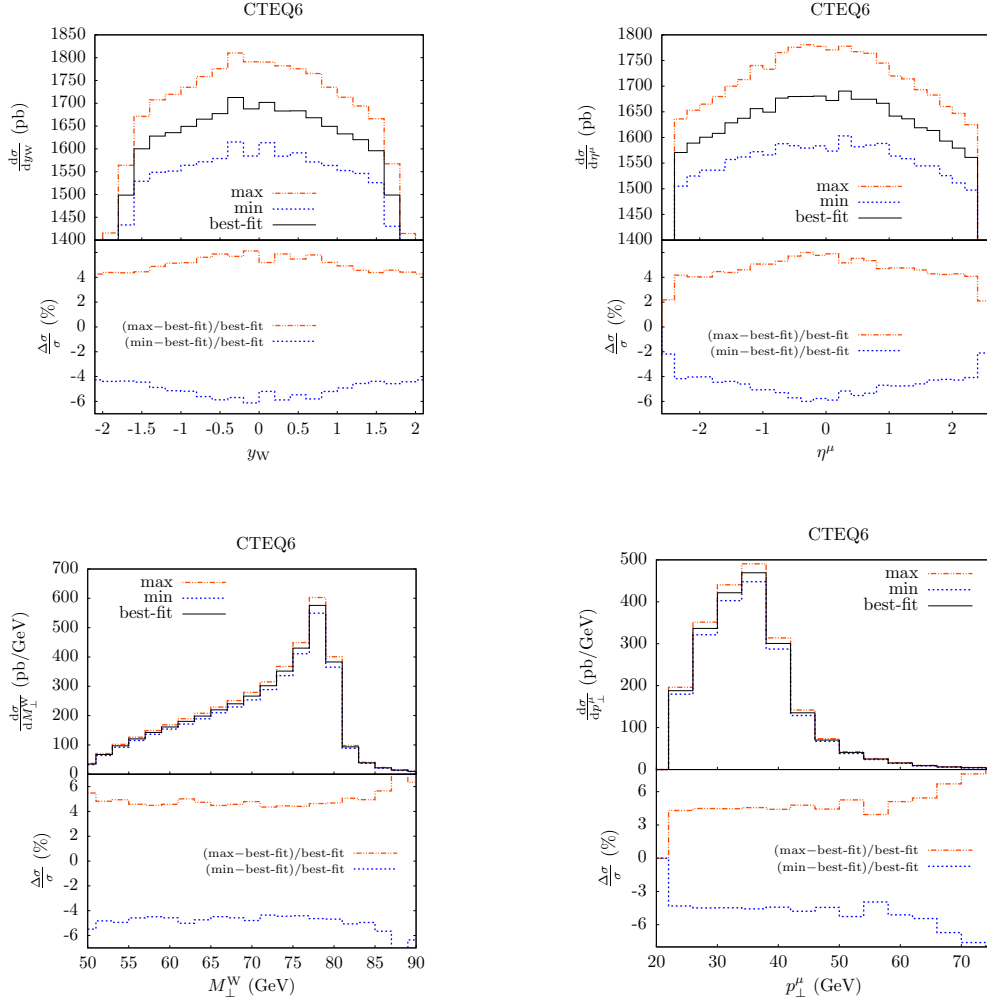


Figure 2: CTEQ61 PDFs uncertainties for W rapidity and muon pseudorapidity (upper plots), and for the W transverse mass and muon transverse momentum (lower plots), according to set up a. at the LHC. In the lower panel of each plot, the relative deviations of the minimum and maximum predicted values w.r.t. the best fit PDF are shown.

where

$$\delta O_i \equiv T \frac{\partial O}{\partial z_i} \approx T \frac{O(z_i^0 + t) - O(z_i^0 - t)}{2t}.$$

n is the number of the error sets (30 for MRST, 40 for CTEQ), T is the tolerance, t is a small step in the space of z_i . Here $O(z_1^0, \dots, z_i^0 \pm t, \dots, z_{n/2}^0)$ is denoted as $O(z_i^0 \pm t)$.

In the lower panel of each plot, the relative deviations of the minimum and maximum predicted values w.r.t. the best fit PDF are shown. As can be seen, the spread of the predictions is at the level of some per cents for all the distributions. In particular, for the W rapidity and muon pseudorapidity the uncertainties vary within 2-4%, reaching their maximum value in the central rapidity region, while for the muon p_\perp and M_\perp^W the relative deviations are about 3-4% around the jacobian peaks, reaching the 6% level in the hard tails of the distributions.

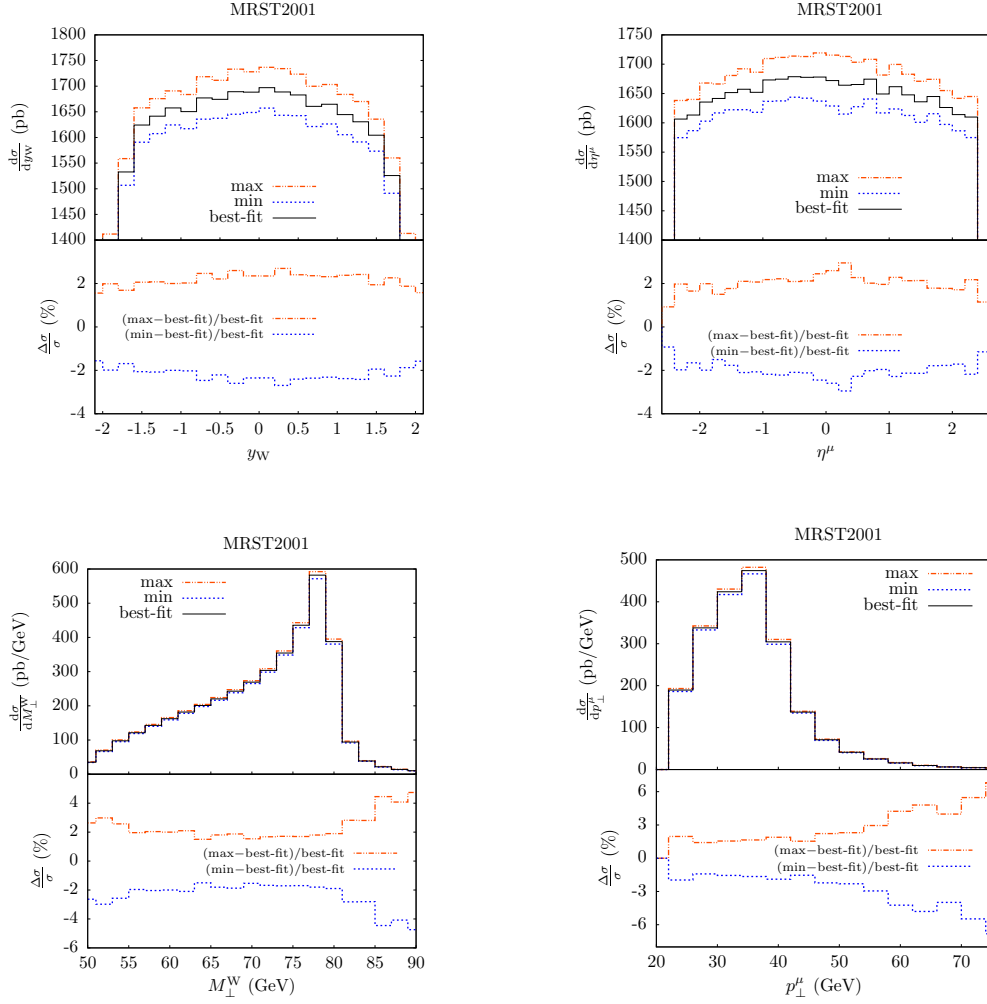


Figure 3: The same as Figure 2 for MRST2001E parameterization.

The same analysis is shown in Figure 3 for the NLO MRST2001E parameterization. The observed uncertainties are smaller by about a factor of two, as expected from the discussion addressed in Section 2.1 about the different values of the tolerance parameter adopted in the two PDF sets.

The results for the W transverse momentum are shown in Figure 4, both for CTEQ61 (left plot) and MRST2001E (right plot). The uncertainties are almost flat in both cases, and of about 3% and 1.5% for CTEQ61 and MRST2001E parameterization, respectively.

We also analyzed the PDF uncertainties on the transverse mass distribution when considering set up b. of Table 2 at the LHC, as shown in Figure 5. We observed that both the CTEQ61 and MRST2001E predictions display deviations w.r.t to the best fit at some per cent level from 1 to 2 TeV, while the uncertainties are, in the average, of the order of 20% in the vicinity of 3 TeV, as due to the well-known gluon PDF uncertainties for large x values dominant in such a region.

It is important to remind, as already remarked, that the estimate of PDF uncertainties

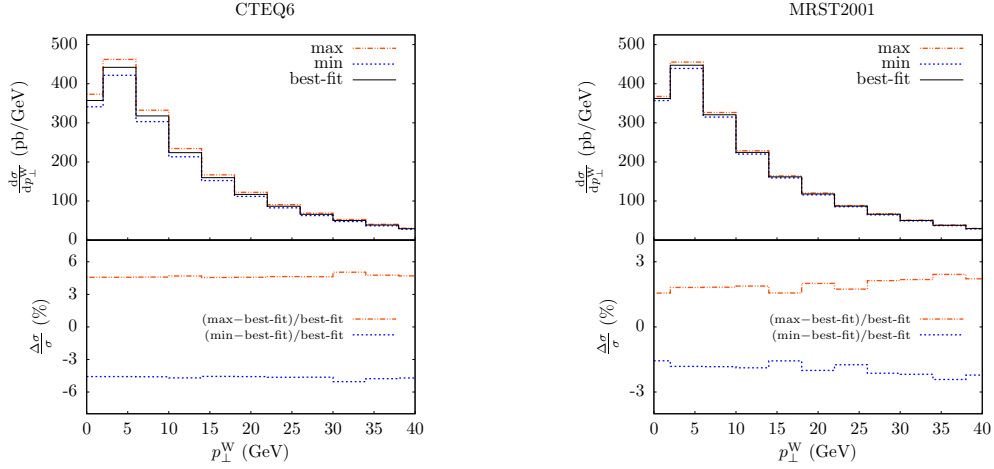


Figure 4: CTEQ61 (left plot) and MRST2001E (right plot) PDFs uncertainties for the W transverse momentum distribution, according to set up a. at the LHC.

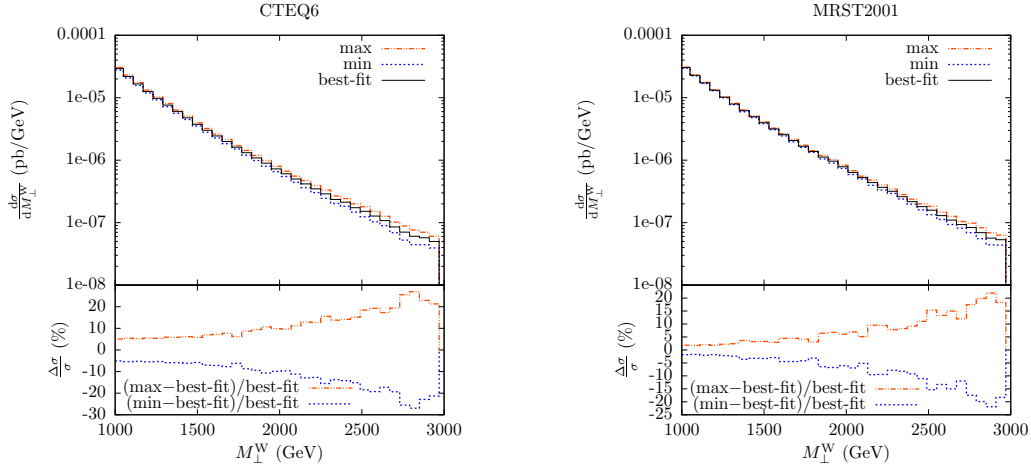


Figure 5: CTEQ61 (left plot) and MRST2001E (right plot) PDFs uncertainties for the W transverse mass in the high tail, according to set up b. at the LHC.

obtained according to such a procedure are of experimental origin only, leaving aside other sources of uncertainty due to theory.

At present the only available set which includes electromagnetic effects in the evolution of the PDFs is MRST2004QED. We have chosen this set to consistently subtract the initial state QED collinear divergences, and also to investigate the contribution of the extra photon-induced partonic subprocesses, due to the presence of a photon density in the proton.

The recent PDFs sets [71, 72, 73] have included new data and a refined treatment of the quark masses effects. These updates turned out to be important for DY phenomenology at the LHC: in fact the total cross sections within cuts change by approximately 3-6% w.r.t. the predictions obtained with the older sets. On top of the overall normalization

variation we observed a moderate (of the order of 1%) but not constant shape change when comparing the transverse mass or the lepton transverse momentum distributions computed with or without massive quark corrections.

Our choice of using MRST2004QED, although it is not the most up-to-date proton parameterization, has been taken to keep the possibility of discussing the relevance of the photon-induced processes, which might be not negligible especially in the searches for new physics signals. For consistency at the Tevatron we have used the Resbos grids based on the CTEQ6.1 PDFs set, which does not include massive charm effects.

The analysis of the present Section is not spoiled by the use of older sets of PDFs nor it does overestimate the uncertainties due to the experimental error from which the PDFs are affected. In fact we numerically checked that the $1\text{-}\sigma$ spread of the predictions obtained with the most recent sets is of the same size, w.r.t. the results shown here.

3.5 Numerical results for the Tevatron

In this section, we present the results obtained for the process $p\bar{p} \rightarrow W^\pm \rightarrow \mu^\pm + X$ at the energy of the Tevatron Run II ($\sqrt{s} = 1.96$ TeV), when imposing the cuts quoted in Table 1. For the various observables of interest, we begin with a discussion of QCD effects, to continue with the analysis of the combination of EW and QCD corrections. The latter is realized according both to the additive formula of eq. (2.1) and the factorized combination as in eq. (2.2). The numerical results presented in the following have been obtained using HORACE including exact NLO EW corrections, but neglecting the contribution of higher-order effects due to multiple photon emission, since the phenomenological impact of these contributions has been already studied in detail, both at the Tevatron and LHC, in a series of previous papers [25, 29, 30, 34]. Moreover, results for the W transverse momentum will not be shown because of the strong sensitivity of this observable to non-perturbative effects, that require a careful modeling and comparison with real data and are, therefore, beyond the scope of the present analysis.

3.5.1 Observables for luminosity monitoring and PDF constraint

After the successful MC tuning at the level of integrated cross sections discussed in Section 3.2, we performed detailed comparisons between the predictions of QCD codes under consideration for those observables of experimental interest to monitor the collider luminosity and to constrain the PDFs.

In Figure 6 we show the results obtained for the W rapidity (left plot) and muon pseudorapidity (right plot) with ALPGEN S_0 , ALPGEN S_2 , MC@NLO and ResBos-A CSS.³ It is important to emphasize that in Figure 6, and in the following plots referring to distributions in the presence of QCD only, the results of all QCD programs have been normalized to the corresponding integrated cross section, in order to point out just the differences in the shape description. In the lower panels of Figure 6 we show the relative deviations of each QCD tool w.r.t. ResBos-A, chosen as a benchmark because of its wide

³As already stated for the integrated cross sections in Section 3.3, the results of ALPGEN S_1 are not shown in Figure 6 and in the next plots for the Tevatron because they are practically indistinguishable from the predictions of ALPGEN S_2 , as we explicitly checked.

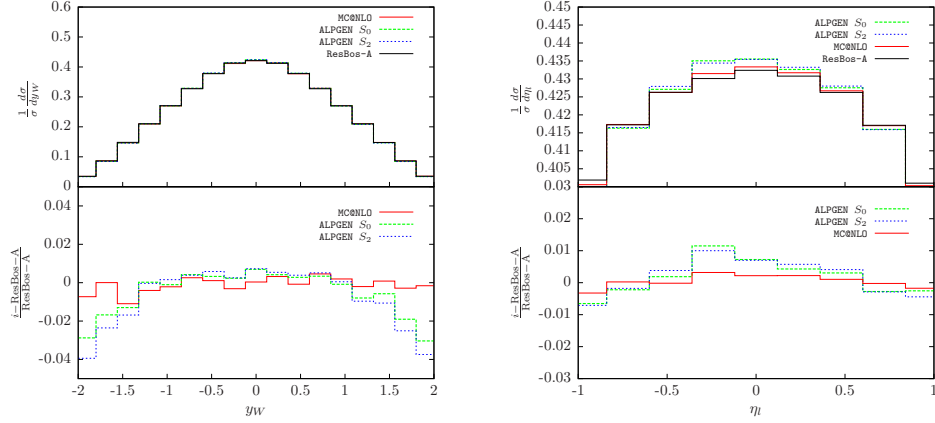


Figure 6: W rapidity (left plot) and muon pseudorapidity (right plot) distributions according to the QCD predictions of ALPGEN S_0 , ALPGEN S_2 , MC@NLO and ResBos-A. In the lower panels the relative deviations of each code w.r.t. ResBos-A are shown.

use at the Tevatron⁴. It can be seen that, in spite of the different theoretical ingredients, the predictions of the QCD programs agree at the $\sim 1\%$ level almost in the whole shape. This can be easily understood because y_W and η_l are rather smooth distributions and, as such, quite insensitive to QCD shape differences, at least for the ranges accessible at the Tevatron.

We also investigated the level of agreement between the QCD codes when considering their predictions for the W charge asymmetry, which is an important quantity at the Tevatron to derive information about the partonic contents of the proton. As can be seen from Figure 7, the absolute differences between the various predictions reach at most the 1% level, again as a consequence of the quite smooth behavior of this distribution.

A first illustration of the combination of EW and QCD corrections at the Tevatron is shown in Figure 8 for the y_W and η_l distributions. The upper panels show the *absolute* predictions obtained by means of the codes ALPGEN S_0 , MC@NLO and according to eq. (2.1), when using MC@NLO⁵ for the simulation of QCD effects in association with HORACE convoluted with HERWIG Parton Shower. In the lower panels, the relative effects in units of ALPGEN S_0 due to QCD (MC@NLO), EW (HORACE_{HERWIG}) and the combination of electroweak and QCD corrections (eq. (2.1)) are shown, as obtained by appropriate combinations of the absolute predictions shown in the upper panel. Strictly speaking, the results referring to MC@NLO+HORACE_{HERWIG} and denoted in the plots as EW correspond to the second term of eq. (2.1), in units of the predictions of ALPGEN S_0 . It can be seen that EW corrections amount to a few per cent negative contribution, QCD NLO effects are of the order of 20%, resulting in a total combined correction of about 15%.

⁴More precisely, the code used at the Tevatron for the modeling of QCD in DY processes is ResBos. However, ResBos-A coincides with ResBos as far as QCD contributions are concerned.

⁵Instead of adopting MC@NLO, the same results could be obtained using ALPGEN with an overall K -factor (defined as σ_{NLO}/σ_{LO}), since the shape predictions of ALPGEN and MC@NLO are in good agreement, as previously shown.

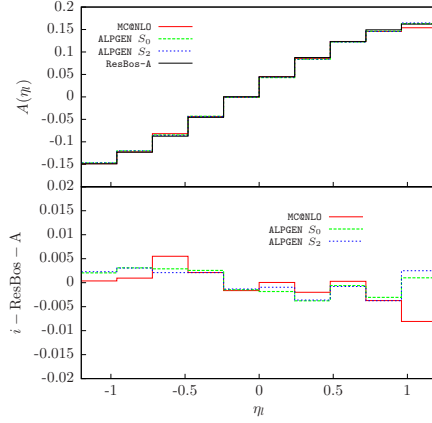


Figure 7: The W charge asymmetry according to the QCD predictions of ALPGEN S_0 , ALPGEN S_2 , MC@NLO and ResBos-A. In the lower panel the absolute deviations of each code w.r.t. ResBos-A are shown.

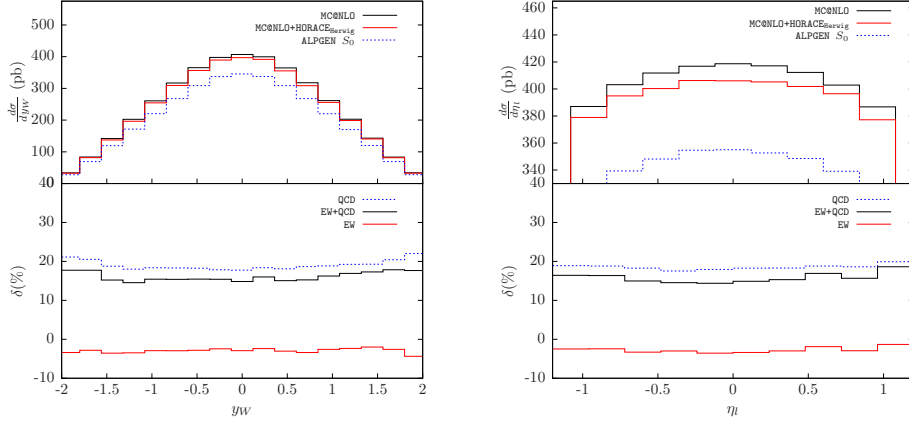


Figure 8: W rapidity (left plot) and muon pseudorapidity (right plot) distributions according to MC@NLO, ALPGEN S_0 and the additive EW+QCD combination. In the lower panels the relative effects due to QCD, EW and EW+QCD corrections are shown in units of ALPGEN S_0 .

We also studied the EW and QCD corrections to the W charge asymmetry and observed that they are of comparable size and tend to sum up, yielding a total correction at the 1% level on the average. We also performed a comparison with ResBos-A, to notice that the predictions of our EW/QCD recipe are in agreement with those of ResBos-A within about 1% in the whole η_l range.

Figure 9 shows the comparison between the additive formula of eq. (2.1) and the factorized prescriptions of (2.2), as normalized to the LO hadron level distributions convoluted with HERWIG PS. The predictions lie in a few per cent band, the factorized prescriptions being quite close to one another. The relative difference between the additive and factorized recipes can be seen as an estimate of the uncertainty due to $\mathcal{O}(\alpha_s^2)$ and $\mathcal{O}(\alpha\alpha_s)$ corrections.

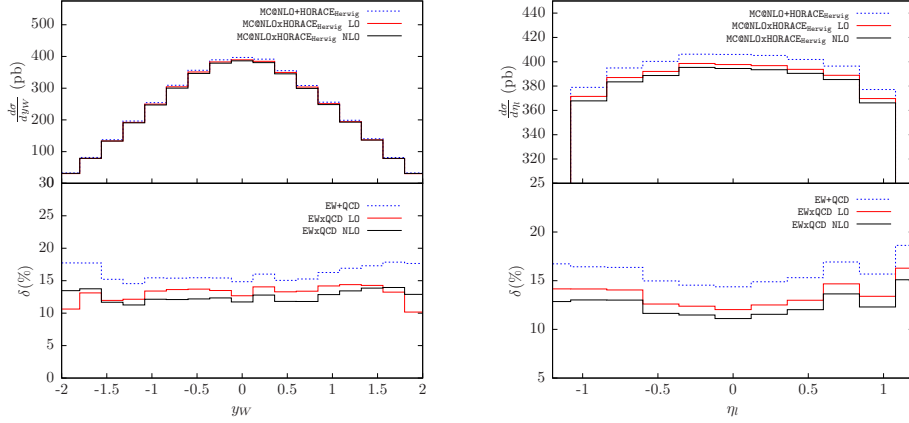


Figure 9: W rapidity (left plot) and muon pseudorapidity (right plot) distributions according to the additive EW+QCD combination and the two EW \otimes QCD factorized prescriptions. In the lower panels the relative effects due to the different combinations are shown in units of ALPGEN S_0 .

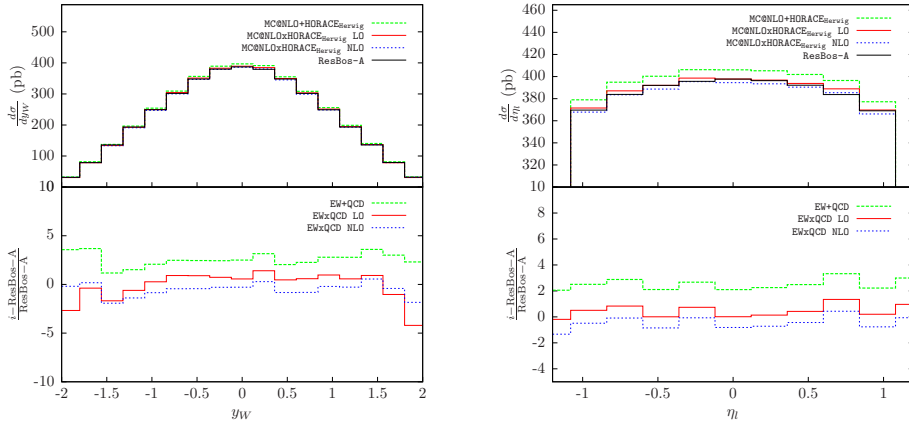


Figure 10: W rapidity (left plot) and muon pseudorapidity (right plot) distributions according to the additive EW+QCD combination, the two EW \otimes QCD factorized prescriptions and ResBos-A. In the lower panels the relative differences of the various combinations w.r.t. ResBos-A are shown.

In figure 10 the absolute predictions of eqs. (2.1) and (2.2) are compared with those of ResBos-A in the upper panel. As can be seen in the lower panels, the relative difference does not exceed the few per cent level, the agreement being better for the factorized prescriptions, consistently with the fact that ResBos-A adopts a factorized formulation as well.

3.5.2 Observables for W precision physics

The status of the QCD predictions for the observables relevant for precision measurements of the W -boson mass is presented in Figure 11, showing the W transverse mass (left plot) and the muon transverse momentum (right plot), according to the results of ALPGEN S_0 , ALPGEN S_2 , MC@NLO and ResBos-A, as in Figure 6 and Figure 7. For such strongly

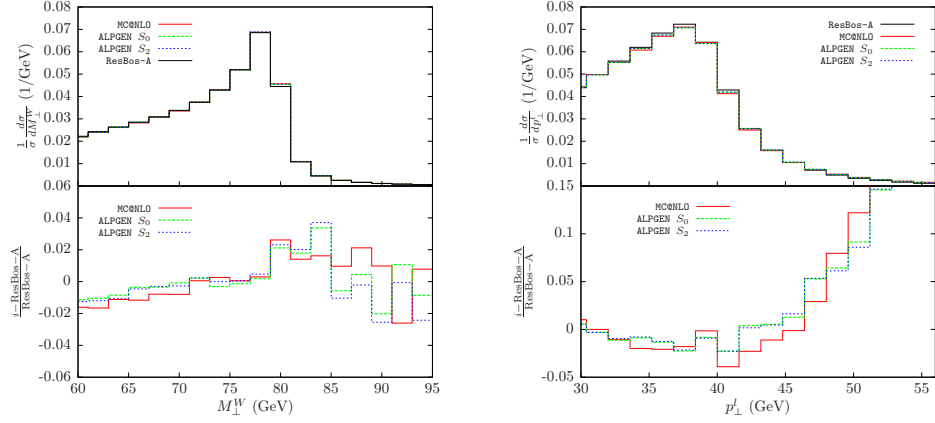


Figure 11: The same as Figure 6 for the W transverse mass (left plot) and muon transverse momentum (right plot) distributions.

varying distributions, it can be noticed that the predictions of the QCD programs differ at some per cent level around the jacobian peak, which is the crucial region for M_W extraction. The relative differences can reach the 5-10% level in the distributions tails. Presumably, the discrepancies around 50 GeV for M_\perp^W and 25 GeV for p_\perp^l have to be ascribed to soft-gluon resummation, which is accurately described in ResBos-A but not taken into account at the same precision level in the other codes. On the other hand, the differences observed around 90 GeV for M_\perp^W and 50 GeV of p_\perp^l are probably due to hard collinear PS effects, which are incorporated in ALPGEN and in MC@NLO but are absent in ResBos-A. Actually, one can notice that in this region the predictions of ALPGEN S_2 and MC@NLO well agree with the pure PS approximation of ALPGEN S_0 , supporting the above interpretation.

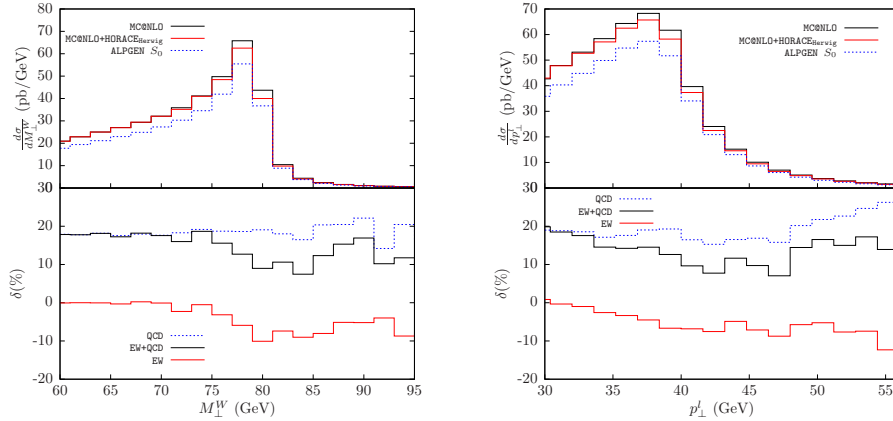


Figure 12: W transverse mass (left plot) and muon transverse momentum (right plot) distributions according to MC@NLO, ALPGEN S_0 and the additive EW+QCD combination. In the lower panels the relative effects due to QCD, EW and EW+QCD corrections are shown in units of ALPGEN S_0 .

A further example of the combination of EW and QCD corrections at the Tevatron is shown in Figure 12 for the M_\perp^W and p_\perp^l distributions. Similarly to Figure 8, the upper

panels show the *absolute* predictions of ALPGEN S_0 , MC@NLO and according to eq. (2.1), while the lower panels illustrate the relative effects due to QCD and EW corrections only and to the combination of electroweak and strong contributions. As can be observed, in the most interesting region around the jacobian peak the NLO corrections are partially compensated by the EW contributions, yielding a total correction of about 10-15%. It is worth noticing that the convolution of EW corrections with the QCD shower changes the shape of EW corrections themselves, smearing them w.r.t. a pure parton-level calculation.

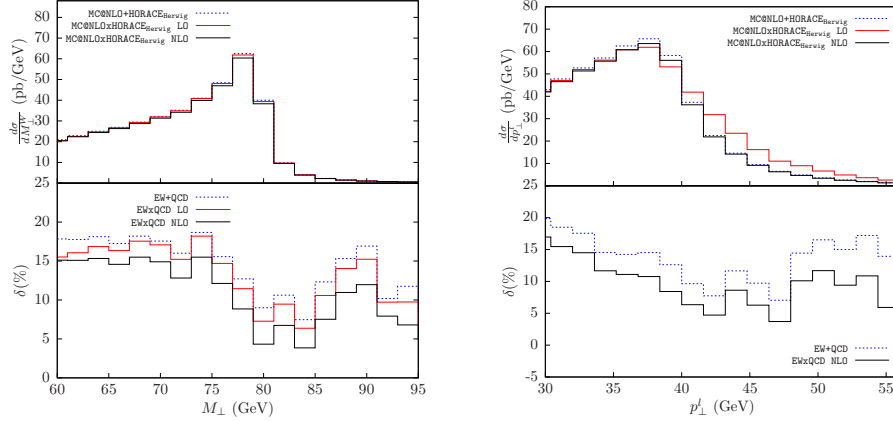


Figure 13: W transverse mass (left plot) and muon transverse momentum (right plot) distributions according to the additive EW+QCD combination and the two $\text{EW} \otimes \text{QCD}$ factorized prescriptions. In the lower panels the relative effects due to the different combinations are shown in units of ALPGEN S_0 .

Figure 13 shows the comparison between the additive formula of eq. (2.1) and the factorized prescriptions of (2.2), as normalized to the LO hadron level distributions convoluted with HERWIG PS. Some comments are in order here. With respect to the case, already discussed, of y_W and η , the differences between the two factorized prescriptions are sizable. In particular, in the case of p_\perp^l , the factorized formula with LO normalization leads to pathological results. This can be understood as due to the fact that NLO corrections are dominated, in the hard p_\perp tail, by $2 \rightarrow 3$ QCD subprocesses not included in a LO calculation. For this kind of observables, the NLO calculation is the first perturbative order able to cover all the relevant phase space regions; hence it is the “lowest order” approximation w.r.t. which evaluate the size of radiative corrections.

Figure 14 shows the comparison between the additive and factorized formulae on the one hand and the ResBos-A prediction on the other one. From the comparison with Figure 11 referring to QCD shape differences only, it can be seen that the trend of the relative deviations is very similar to that observed between the results of MC@NLO and ResBos-A, while the size of the differences increases of some per cents in the tails, as a consequence of the inclusion of the normalization in the codes predictions. It can also be noticed that the differences between the two approaches are largely dominated by QCD effects. Therefore, as already remarked about Figure 11, the differences below the peaks are probably due to soft-gluon resummation effects. On the other hand, the discrepancies present above

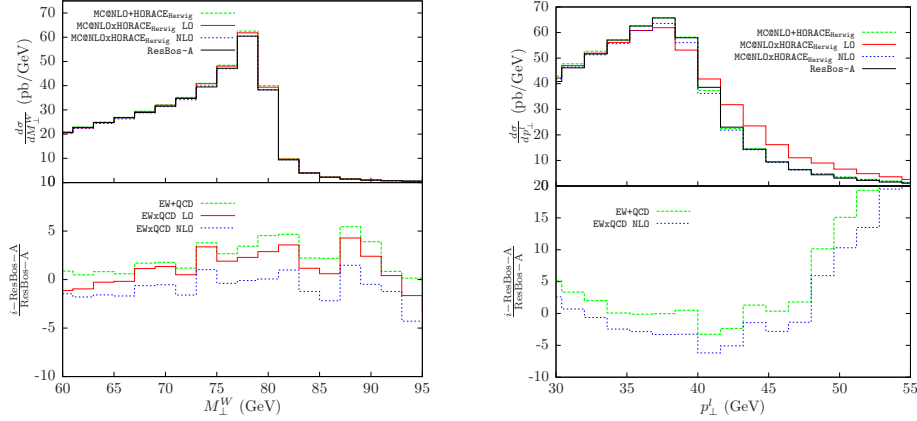


Figure 14: W transverse mass (left plot) and muon transverse momentum (right plot) distributions according to the additive EW+QCD combination, the two EW \otimes QCD factorized prescriptions and ResBos-A. In the lower panels the relative differences of the various combinations w.r.t. ResBos-A are shown.

the peaks have to be presumably ascribed to hard collinear PS contributions taken into account in our calculation but not implemented in ResBos-A. To better understand the origin of these differences, it would be interesting to perform comparisons with the predictions of ResBos-A when taking into account the effect of finite order QCD contributions (the so-called Y terms) in its formulation. Unfortunately, no public grids are available for such theoretical configuration. Concerning the EW contributions, the two programs essentially predict the same quantitative effects. This is not unexpected because EW corrections in the vicinity of the W peak are largely dominated by final-state QED radiation, as widely discussed in the literature, and therefore the inclusion of exact NLO corrections in HORACE versus the approximation limited to the inclusion of NLO final-state QED corrections in ResBos-A translates into differences at the 0.1% level, as we explicitly checked. As a whole, it is worth stressing that closely around the jacobian peak the additive recipe and ResBos-A show differences of a few per cent, for both M_{\perp}^W and p_{\perp}^l , whereas the factorized NLO prescription exhibits smaller deviations in the M_{\perp}^W case. Such differences could be relevant in view of the future measurements of the W mass with ~ 20 MeV precision at the Tevatron and should be further scrutinized on the experimental side. In particular, the combination of MC@NLO with HORACE, as adopted in this study, could be used to cross-check the precision measurement of the W -boson mass as currently obtained in terms of the generators ResBos (for QCD effects) and HORACE, PHOTOS [32] and WGRAD (for EW corrections).

Results for photon-induced processes at the Tevatron are not shown since they are negligible because of the very small photon content inside the proton for the typical x values probed by DY kinematics at the Tevatron.

3.6 Numerical results for the LHC

In this section, we present the results obtained for the process $pp \rightarrow W^{\pm} \rightarrow \mu^{\pm} + X$ at

the LHC ($\sqrt{s} = 14$ TeV), when imposing the cuts quoted in Table 2. As for the Tevatron analysis, we begin with a discussion of QCD effects on the relevant observables (considering shape predictions only), to continue with the study of the combination of EW and QCD corrections. Results taking into account higher-order leading log QED corrections and predictions for the W transverse momentum observable will not be given in the following, for the same reasons already emphasized at the beginning of Section 3.5.

3.6.1 Observables for luminosity monitoring and PDF constraint

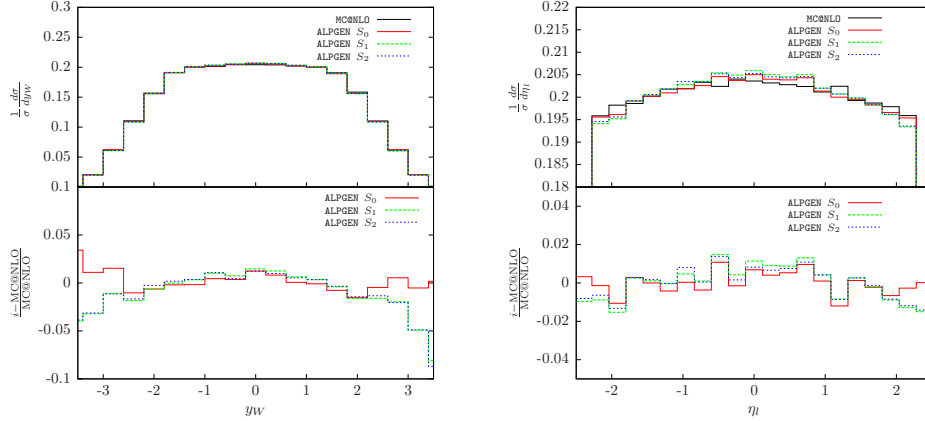


Figure 15: W rapidity (left plot) and muon pseudorapidity (right plot) distributions according to the QCD predictions of ALPGEN S_0 , ALPGEN S_1 , ALPGEN S_2 and MC@NLO. In the lower panels the relative deviations of each code w.r.t. MC@NLO are shown.

In Figure 15 we show the results obtained for the W rapidity (left plot) and muon pseudorapidity (right plot) with the QCD generators ALPGEN S_0 , S_1 and S_2 , and MC@NLO, considering set up a. in Table 2. In the lower panels we show the relative deviations of the ALPGEN variants w.r.t. MC@NLO. It can be noticed that, while for η_l the relative differences between ALPGEN and MC@NLO are at a few per cent level in the whole range, for the W rapidity the agreement in the shape predicted by the two generators is quite satisfactory (at the 1% level) in the central region, but it deteriorates in the very forward and very backward limits, that anyway marginally contribute to the integrated cross section. In particular, in these regions, the pure PS predictions represented by ALPGEN S_0 indicate a quite smooth excess of events w.r.t. MC@NLO, while the (practically indistinguishable) deviations of ALPGEN S_1 and of ALPGEN S_2 w.r.t. MC@NLO have a more pronounced opposite trend.

The interplay between EW and QCD corrections at the LHC is shown in Figure 16 for the y_W and η_l distributions. The upper panels show the *absolute* predictions of MC@NLO, ALPGEN S_0 , MC@NLO+HORACE (additive combination) and MC@NLO \otimes HORACE (factorized combination) interfaced to HERWIG PS. In the lower panels, the relative effects due to the combination of EW and QCD corrections, as well as for the EW and QCD contributions separately, are shown. The size of NLO EW and QCD corrections is almost the same as the one seen for the Tevatron in Figure 8. In particular, the negative NLO EW

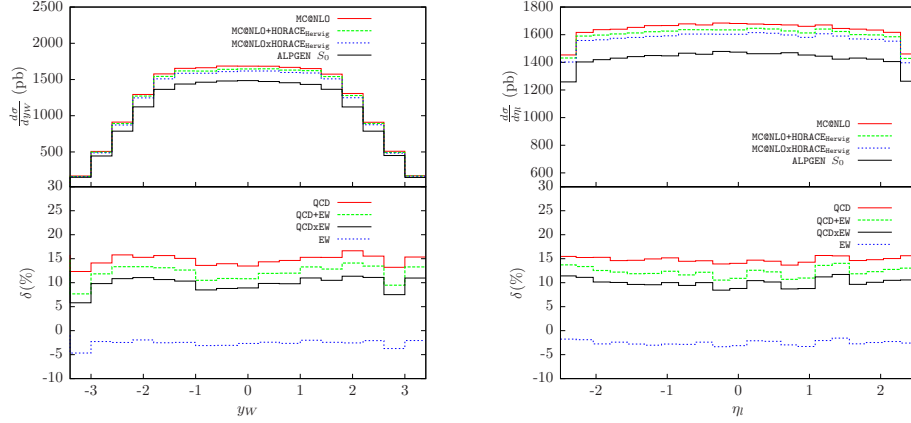


Figure 16: W rapidity (left plot) and muon pseudorapidity (right plot) distributions according to the predictions of MC@NLO, ALPGEN S_0 , MC@NLO+HORACE and MC@NLO \otimes HORACE. In the lower panels the relative effects due to QCD, EW and combined corrections are shown in units of ALPGEN S_0 .

effects partially cancel the positive contribution due to NLO QCD corrections, resulting into combined EW and QCD corrections at the 10% level, for both y_W and η_l and for both additive and factorized prescriptions. Hence, the interplay between EW and QCD contributions is crucial for precise simulations of the observables relevant for luminosity monitoring and PDF constraint at the LHC.

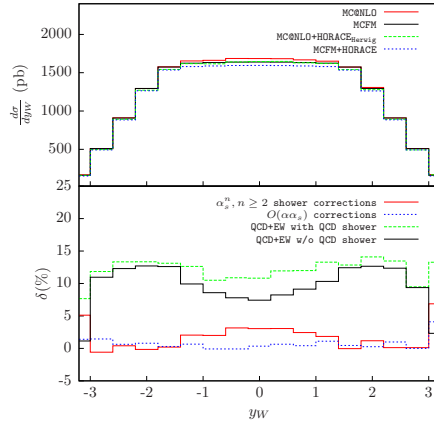


Figure 17: W rapidity distribution according to the predictions of MCFM, MC@NLO, MCFM+HORACE and MC@NLO+HORACE_{HERWIG}. In the lower panel the relative effects due to $O(\alpha_s^2)$ QCD corrections, $O(\alpha_s)$ mixed corrections and QCD+EW corrections with and without QCD showering.

As remarked in Sect. 2.4, both the additive and factorized combination of EW and QCD corrections contain, beyond the very same $O(\alpha)$ and $O(\alpha_s)$ content, higher-order contributions dominated by $O(\alpha_s^2)$ and mixed $O(\alpha\alpha_s)$ corrections. It is therefore interesting to analyze how these higher-order corrections compare to each other. Since such higher-

order effects originate, in both the additive and factorized recipe, from the QCD PS and the convolution of the QCD PS with the NLO predictions, a simple strategy to disentangle the relative effect of $O(\alpha_s^2)$ and $O(\alpha\alpha_s)$ corrections is to compare the predictions of the combination of pure NLO codes (lacking, by construction, the contribution of the QCD shower evolution) with those of one of the two recipes described in Sect. 2.4 or their variants. An example of such a study is given for y_W in Fig. 17, where, for definiteness, the results of the additive recipe MC@NLO + HORACE_{HERWIG} are compared with those of the pure NLO combination MCFM + HORACE, as well as with the predictions of the "intermediate" theoretical formulations given by MC@NLO + HORACE (missing mixed $O(\alpha\alpha_s)$ corrections) and MCFM + HORACE_{HERWIG} (missing $O(\alpha_s^2)$ shower effects). As it can be seen from the lower panel, the fixed NLO predictions of MCFM + HORACE differ from those of MC@NLO + HORACE_{HERWIG} at the some per cent level, showing the overall importance of QCD shower and mixed EW-QCD corrections for a precise simulation of the y_W distribution. It can be also noticed that $O(\alpha\alpha_s)$ corrections are very small, while QCD shower corrections amount to a few per cent, thus dominating the EW-QCD combination for this observable.

3.6.2 Observables for W precision physics

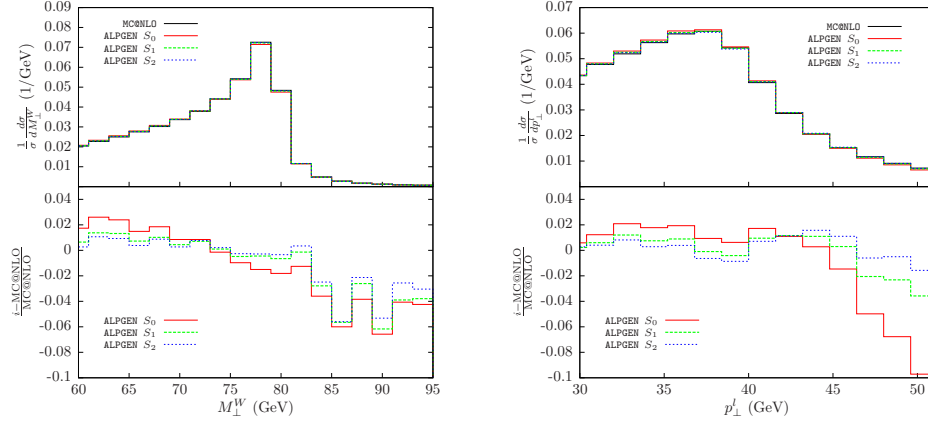


Figure 18: W transverse mass (left plot) and muon transverse momentum (right plot) distributions according to the QCD predictions of ALPGEN S_0 , ALPGEN S_1 , ALPGEN S_2 and MC@NLO. In the lower panels the relative deviations of each code w.r.t. MC@NLO are shown.

The QCD predictions for the W transverse mass and muon transverse momentum according to set up a. of Table 2 is shown in Figure 18. The results of different variants of the ALPGEN generator are compared with the predictions of MC@NLO. As can be seen from the lower panels, the agreement in the shape predicted by the two generators is very satisfactory (at the 1% level) around the jacobian peak, while the relative deviations reach the 5-10% level in the hard tail of both M_\perp^W and p_\perp^l spectrum. In particular, it can be noticed that for M_\perp^W the relative difference of ALPGEN S_0 w.r.t. MC@NLO has the same size and shape of the deviations observed for the predictions of ALPGEN S_1 and of ALPGEN S_2 , while this is not the case for the hard p_\perp^l tail, where the MC@NLO predictions

are in better agreement with the ALPGEN versions including matched matrix-elements corrections rather than with ALPGEN S_0 . This can be easily understood in terms of the rather smooth dependence of the M_{\perp}^W distribution from QCD corrections, at variance of the pronounced sensitivity of p_{\perp}^l from hard QCD radiation. The importance of the latter is particularly visible in Figure 19, showing the predictions of the QCD generators for the muon transverse momentum distribution up to 80 GeV. Actually, one can see the well-known fact [58] that in the high tail of such distribution, i.e. above ~ 50 GeV, there is an important enhancement due to NLO and matched matrix elements corrections w.r.t. the QCD PS approximation represented by ALPGEN S_0 . Furthermore, a substantial agreement between the shape predicted by MC@NLO and the ones obtained with ALPGEN S_1 and ALPGEN S_2 is observed, although a closer inspection reveals discrepancies above ~ 50 GeV in the 10% range, as illustrated in the lower panel of Figure 19, where however the cross section is quite small and the relative statistics quite limited. As a whole, the deviations between MC@NLO and ALPGEN in its different flavors shown in Figure 18 and Figure 19 can be ascribed to the different matching procedures between real and virtual QCD radiation implemented in the two generators.

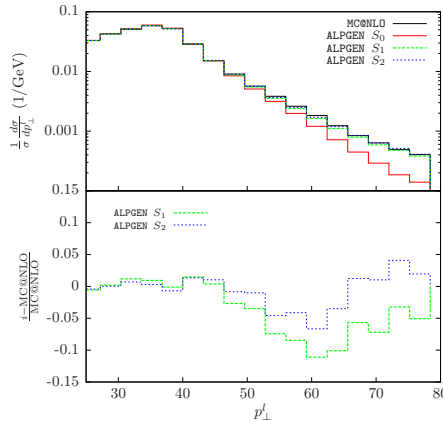


Figure 19: The muon transverse momentum distribution up to 80 GeV according to the QCD predictions of ALPGEN S_0 , ALPGEN S_1 , ALPGEN S_2 and MC@NLO. In the lower panels the relative deviations of ALPGEN S_1 and ALPGEN S_2 w.r.t. MC@NLO are shown.

Because of the importance of precise predictions for the M_W determination from fits to M_{\perp}^W and p_{\perp}^l , we show in Figure 20 the W transverse mass (left plot) and muon transverse momentum (right plot) distributions according to the QCD predictions of MC@NLO, when varying the renormalization/factorization scale from its default value $\mu_0 = \mu_R = \mu_F = \sqrt{p_{\perp W}^2 + M_W^2}$ to $\mu_0/2$ and $2\mu_0$. As it can be seen from the lower panels in Figure 20, the scale variations induce relative differences w.r.t. the default choice at a few per cent level for both the distributions, without modifying the shape of the distributions themselves. These deviations reflect the $\sim \pm 3\%$ variations obtained for the cross sections by integrating the above distributions by MC@NLO, given by 8026(5) pb for $\mu = \mu_0/2$, 8254(5) pb for $\mu = \mu_0$ and 8502(5) pb for $\mu = 2\mu_0$.

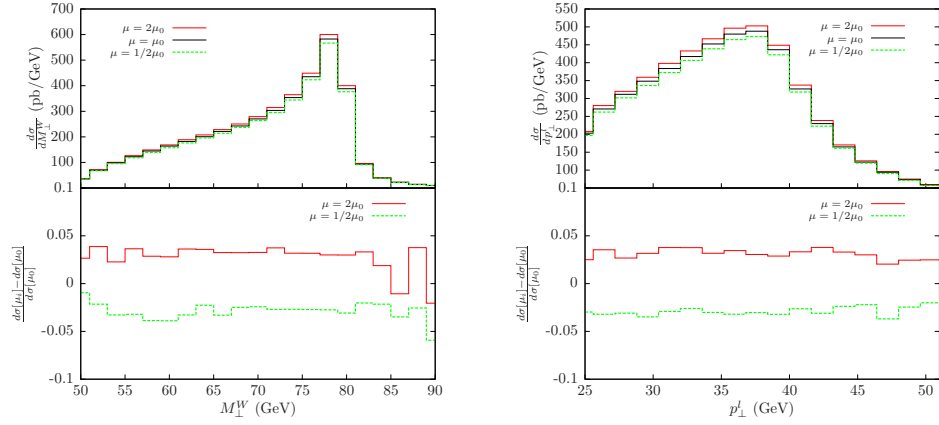


Figure 20: W transverse mass (left plot) and muon transverse momentum (right plot) distributions according to the QCD predictions of MC@NLO for renormalization/factorization scale μ at its default value μ_0 given in the text and for $\mu = 1/2\mu_0, 2\mu_0$. In the lower panels the relative deviations due to scale variations w.r.t. the default choice are shown.

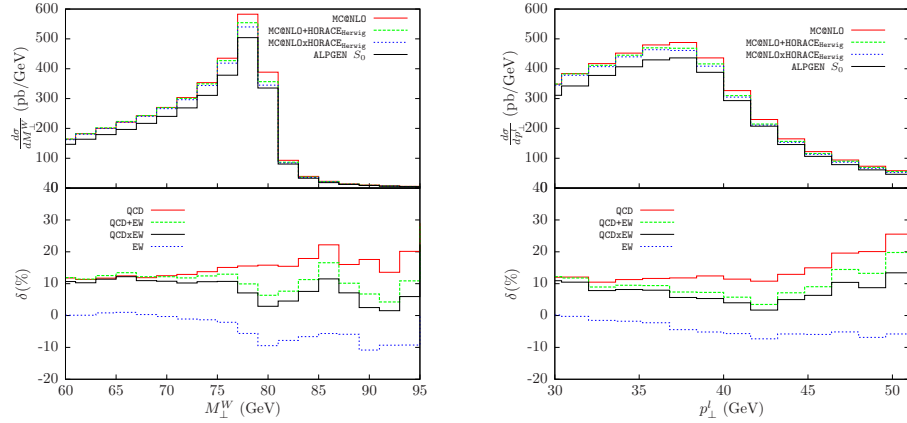


Figure 21: The same as Figure 16 for the W transverse mass distribution (left plot) and muon transverse momentum (right plot).

The combined effect of EW and QCD contribution at the LHC is illustrated in Figure 21. The upper panels show the predictions of the generators ALPGEN S_0 , MC@NLO, MC@NLO + HORACE and MC@NLO \otimes HORACE. The lower panels illustrate the relative effects of NLO QCD and EW corrections, as well as their combination. From fig. 21 it can be seen that the NLO QCD corrections are positive and tend to compensate the effect due to EW corrections. Therefore, their interplay is unavoidable for a precise M_W extraction at the LHC, yielding an overall correction of about 5-10% close to the peaks for both the additive and factorized prescriptions. As already stressed for such distributions at the Tevatron, it is also worth noticing that the relative size and shape of EW corrections to M_W^T and p_T^l is modified by the convolution with QCD shower evolution, as can be inferred from comparison with the results for pure EW contributions existing in the literature.

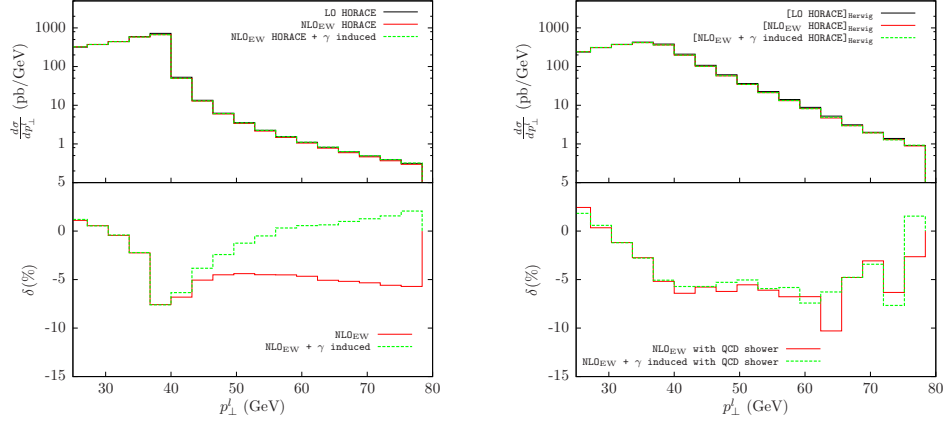


Figure 22: Electroweak and γ -induced corrections without (left) and with (right) QCD shower evolution to the lepton transverse momentum distribution.

This indicates that a naive combination of QCD and EW corrections, in the absence of QCD shower evolution on top of EW effects, is rather inadequate for precise simulation of physical observables. This feature is remarked in Figure 22, showing the relative effect of EW corrections and photon-induced processes for the lepton p_\perp distribution in the absence of QCD parton shower convolution (left plot) and in the presence of QCD shower evolution (right plot). In particular, it can be noticed that the some per cent enhancement due to the γ -induced processes in the hard tail of the p_\perp^l distribution without QCD shower largely disappears when the EW effects are convoluted with QCD shower radiation.

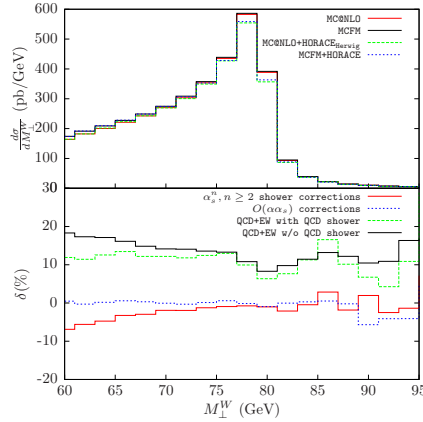


Figure 23: The same as Fig. 17 for the W transverse mass distribution.

An inspection of the relative impact due to $O(\alpha_s^2)$ and mixed $O(\alpha\alpha_s)$ corrections analogous to that shown in Fig. 17 for y_W is shown in Fig. 23 for the transverse mass distribution. For this observable, it can be seen that the QCD shower evolution is particularly important below the Jacobian peak, where it introduces corrections of some per cent, while mixed EW-QCD contributions are not negligible above it. More importantly, a naive combina-

tion of QCD and EW corrections, omitting the contribution of QCD shower, appears to be inadequate for a precision calculation of M_T^W , as the clearly visible difference between the predictions of MC@NLO + HORACE_{HERWIG} and of MCFM + HORACE points out. It follows immediately that a measurement of the W mass at the LHC with an aimed accuracy of a few MeV must necessarily rely upon MC generators including combined QCD and EW corrections according to the highest theoretical standards.⁶

3.6.3 Observables for new-physics searches

The numerical results corresponding to the distributions interesting for the search for new physics at the LHC are shown in Figure 24 and Figure 25 for what concerns QCD predictions, and in Figure 26 and Figure 27, for the combination of EW and QCD corrections. The simulations have been performed using the cuts referring to set up b. of Table 2 and imposing additional jet veto conditions for what concerns the results shown in Figure 27.

Concerning Figure 24, it can be seen that the shape predicted by the different variants of ALPGEN w.r.t. the one obtained with MC@NLO has a very similar trend for both M_\perp^W in the range 1-2 TeV and p_\perp^l in the region 0.5-1 TeV. The predictions of all the ALPGEN versions, both without and with matrix element corrections, nicely agree with the MC@NLO results within a 5% band.

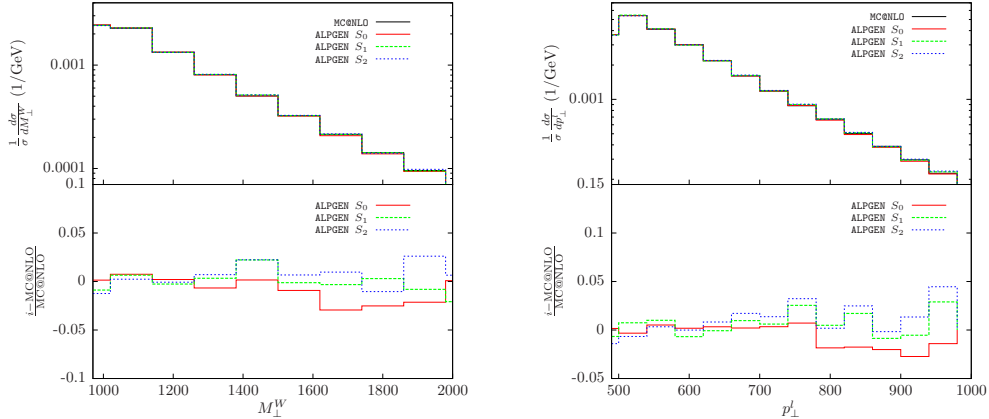


Figure 24: The same as Figure 18 for the transverse mass (left plot) and lepton transverse momentum (right plot) distributions in the very high tails, according to set up b. at the LHC.

Figure 25 shows the W transverse mass (left plot) and muon transverse momentum (right plot) distributions according to the QCD predictions of MC@NLO, when varying the renormalization/factorization scale from its default value $\mu_0 = \mu_R = \mu_F = \sqrt{p_{\perp W}^2 + M_W^2}$ to $\mu_0/2$ and $2\mu_0$. As can be seen from the lower panels, the scale variations induce relative differences w.r.t. the default choice of a few per cent around 1 TeV for M_\perp^W , reaching

⁶It is worth noticing that for the first bins close to the kinematical boundary ($M_T^W = 50$ GeV, not shown in the figure) the prediction by MCFM is negative. This is a well known effect already discussed in [42, 94], and due to perturbative instabilities of the NLO calculation. As a consequence, the results by MCFM around the jacobian peak appear to be slightly larger than the corresponding ones by MC@NLO, without contradicting the results for the integrated cross sections shown in Tab. 7.

O(-10%) at 3 TeV, but where the cross section is two orders of magnitude smaller. For p_\perp^l the scale variations are milder, always within $\pm 5\%$.

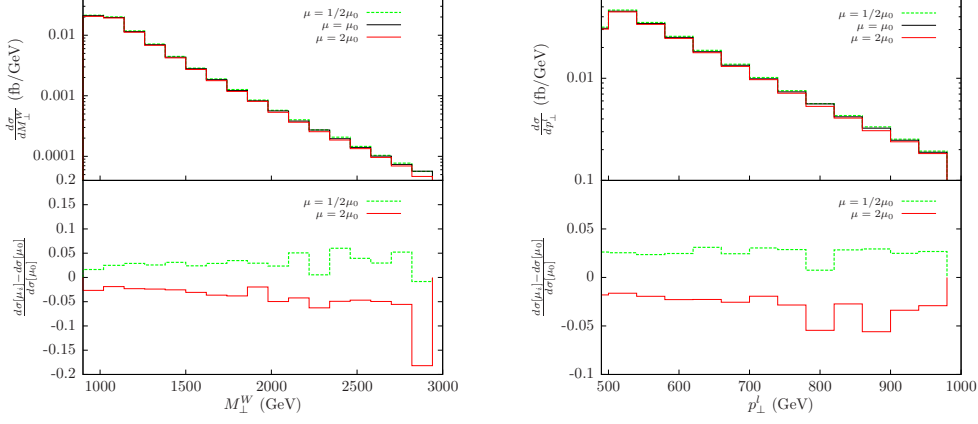


Figure 25: The same as Figure 20 for the transverse mass (left plot) and lepton transverse momentum (right plot) distributions in the very high tails, according to set up b. at the LHC.

The interplay between QCD and EW corrections in the high tail of M_\perp^W and p_\perp^l distributions is shown in Figure 26 (for the standard cuts of set up b. in Table 2) and Figure 27 (when including additional jet veto conditions).

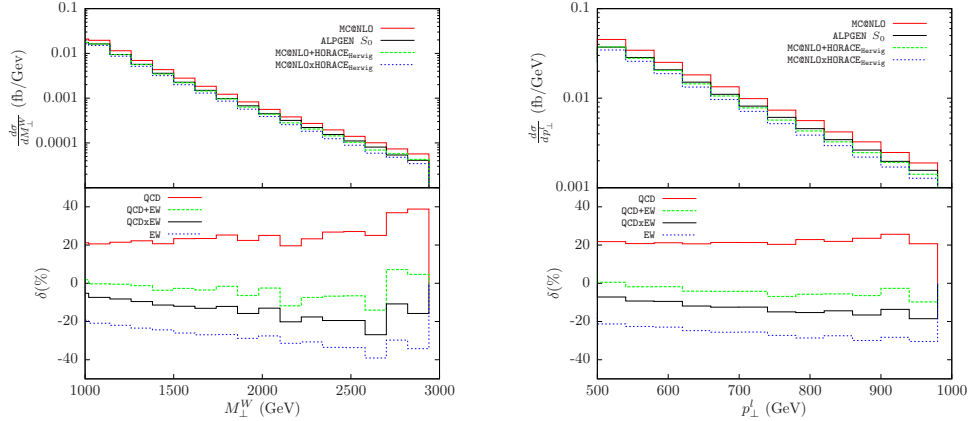


Figure 26: The same as Figure 21 for the transverse mass (left plot) and lepton transverse momentum (right plot) distributions in the high tails, according to set up b. at the LHC.

The jet veto conditions have been implemented by vetoing any hard jet with $p_\perp > 30$ GeV in the central rapidity region ($|y_{\text{jet}}| < 2.5$). In both cases, and for both M_\perp^W and p_\perp^l , NLO QCD corrections are positive (of the order of 20-40% for standard cuts and between 20-60% in the presence of jet veto requirements) and combine with very large negative EW Sudakov logarithms. When imposing standard selection criteria, their factorized combination is about $-10(+10)\%$ for $M_\perp^W \simeq 1.5(3)$ TeV and about $-5(-20)\%$ for $p_\perp^l \simeq 0.5(1)$ TeV, the additive combination yielding smaller effects. Therefore, a precise

normalization of the SM background to new physics searches necessarily requires the simultaneous control of QCD and EW corrections, as also pointed out in [15] for the NC DY process in the high invariant mass region, where a similar compensation between strong and EW contributions takes place. It is worth noticing that in such a region the large negative Sudakov virtual logarithms can be compensated by real weak boson emission, as pointed out in [95]. Concerning the inclusion of two-loop EW Sudakov logarithms, whose calculation is available in the literature [96, 97, 98], it should be considered in view of a theoretical accuracy at the percent level. For the same reason it should be accompanied by the simultaneous control of the NNLO QCD corrections.

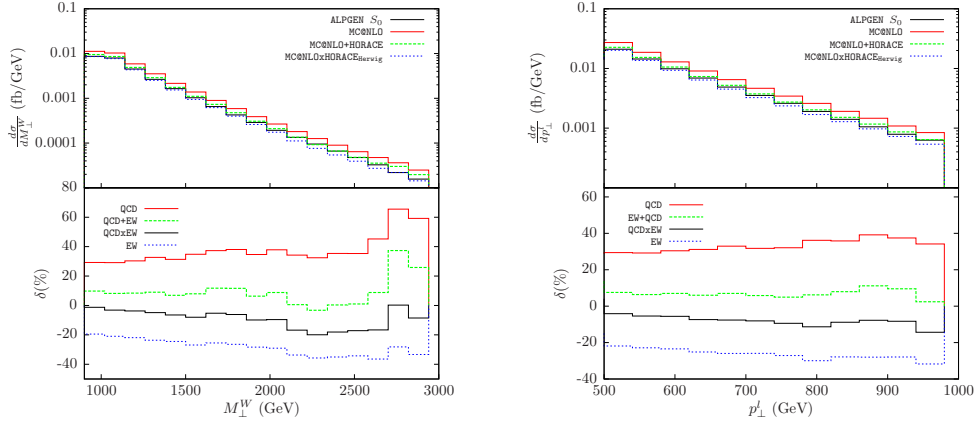


Figure 27: The same as Figure 21, according to set up b. at the LHC and in the presence of additional jet veto conditions.

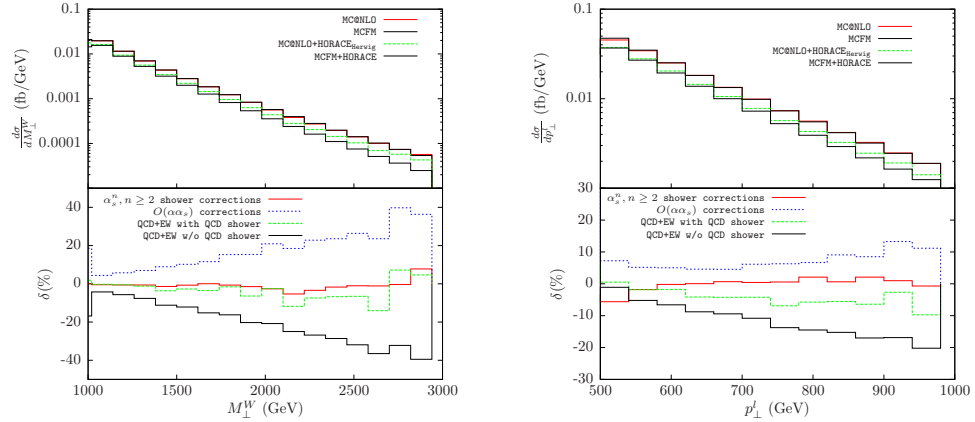


Figure 28: The same as Figure 17 for the transverse mass (left plot) and lepton transverse momentum (right plot) distributions in the high tails, according to set up b. at the LHC.

As done for y_W and M_T^W in the presence of the standard analysis cuts denoted as LHCa, we also investigated how the predictions of a combination of pure NLO codes for EW and QCD corrections compare with those in which QCD shower effects are taken into

account when considering M_T^W and p_T^l in the set up LHC b. The results of this study are shown in Fig. 28 for M_T^W (left plot) and p_T^l (right plot). It can be seen that the pure NLO results differ from those including QCD shower contributions at the 10% level for p_T^l and even more, between 20-30%, for M_T^W in the very hard tail. This important difference is due to the presence of large EW Sudakov logarithms in the NLO EW calculation, giving rise to sizable $O(\alpha\alpha_s)$ corrections at the NNLO level. Hence, the evaluation of the DY background to new physics searches in this region should take carefully under control the combined effect of QCD-EW corrections, especially in the event new physics would manifest as a moderate modification of the DY continuum, rather than as a clearly visible resonance.

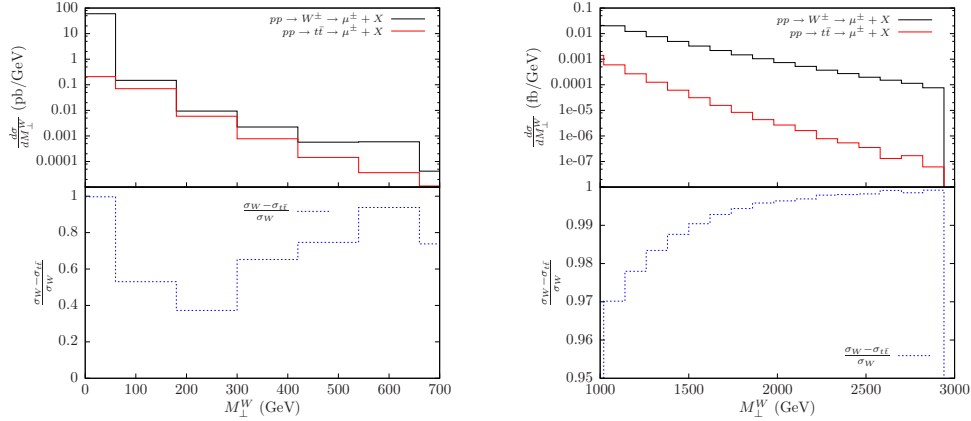


Figure 29: Upper panels: transverse mass distribution of the single W production process (black histogram) and of the $t\bar{t}$ process (red histogram), according to the event selection specified in the text. Lower panels: relative difference of the two contributions, for two transverse mass windows.

To complete the phenomenological analysis, we also performed an investigation of the contribution to the transverse mass due to the top -pair production process $pp \rightarrow t\bar{t} \rightarrow \mu^\pm + X$ (simulated with ALPGEN) in comparison with $pp \rightarrow W^\pm \rightarrow \mu^\pm + X$. The obtained results are shown in Figure 29, for a moderate transverse mass range up to 700 GeV (left plot) and in the high tail up to 3 TeV (right plot). For the $t\bar{t}$ process, all the t leptonic decays are simulated and the events are considered as contributions to the signature when at least a muon is present in the final state. Whenever just a single muon is part of the final state products, the W transverse mass is reconstructed in terms of its transverse momentum, whereas in the case two muons are present the W transverse mass is calculated in terms of the leading- p_t muon. The unobserved X state consists of the two b -quarks and two neutrinos coming from the top and W decays, respectively. The missing transverse momentum entering the definition of W transverse mass is obtained by summing over the missing p_t of the two neutrinos and requiring for each of the two the condition $\cancel{E}_T \geq 25$ GeV, consistently with the cuts imposed in the analysis of W production events. As can be seen from Figure 29, the $t\bar{t}$ process gives, for the event selection assumed, a sizable (of the order of several tens per cent) contribution to the $\mu^\pm + X$ signature in the transverse mass range between about 100 GeV and 600 GeV, while it is at a few per cent level in the high tail.

3.7 Results for jet multiplicity (Tevatron and LHC)

We conclude our phenomenological study with the presentation of the results concerning the distributions of the number of jets, showing the predictions obtained for the Tevatron in comparison with those valid for the LHC. The jets are required to satisfy the following cuts: $E_{Tj} > 20$ GeV, $|\eta_j| < 5$, $\Delta R_{ij} > 0.7$, where ΔR_{ij} is the separation between the i -th and j -th jet in the $\eta - \phi$ plane. Jets are reconstructed by means the cone algorithm provided by the GETJET package [99], which represents a simplified jet cone algorithm a la UA1 (for the sake of simplicity, we stop the evolution at the shower level).

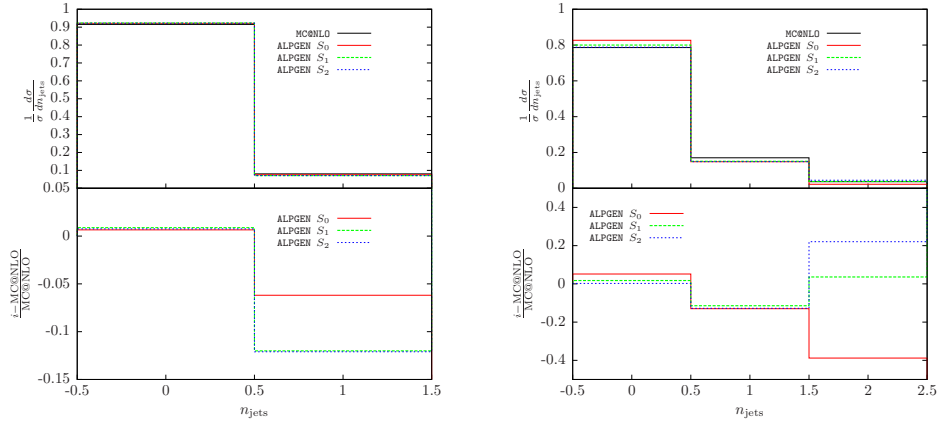


Figure 30: QCD predictions of ALPGEN S_0 , ALPGEN S_1 , ALPGEN S_2 and MC@NLO for the number of jets distribution at the Tevatron (left plot) and at the LHC, set up a. (right plot). In the lower panels the relative deviations of each code w.r.t. MC@NLO are shown.

From the QCD generators used in our analysis, the predictions for the number of jets distribution are shown in Figure 30 for the Tevatron (left plot) and the LHC (right plot), set up a. At the Tevatron energies, about 90% of single W production events are without any extra real hard QCD radiation, while the fraction of events with one additional jet is about 10%. At the LHC, the sharing of the events is, not unexpectedly, quite different: about 80% of the events do not contain extra jets, the fraction of events with one additional jet is slightly smaller than 20%, while events with at least two additional jets amount to a few per cent. As it can be seen from the lower panels in Figure 30, there is good agreement between the predictions of MC@NLO and ALPGEN variants for the W production rate without any extra jet both at the Tevatron and LHC. At the Tevatron, for the events with one additional jet, MC@NLO predictions differ from ALPGEN S_0 results (where the additional jet is generated through the PS cascade) at the 5% level and from ALPGEN S_1 and ALPGEN S_2 predictions at the $\sim 10\%$ level. At the LHC, all the ALPGEN variants provide results differing from the MC@NLO ones at the $\sim 10\%$ level for events with one extra jet, while for the fraction of two additional jet events there is good agreement between MC@NLO and ALPGEN S_1 but significant deviations are present between MC@NLO and either ALPGEN S_0 or ALPGEN S_2 , as expected.

In Figure 31 we show the number of jets distribution corresponding to set up b. at the

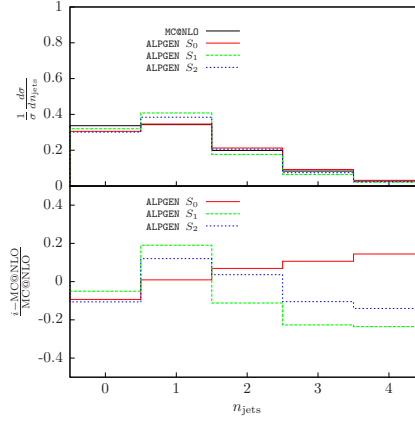


Figure 31: QCD predictions of ALPGEN S_0 , ALPGEN S_1 , ALPGEN S_2 and MC@NLO for the number of jets distribution at the LHC, set up b. In the lower panels the relative deviations of each code w.r.t. MC@NLO are shown.

LHC. As can be seen, the requirement $M_{\perp}^W > 1$ TeV changes very significantly the number of jets distribution w.r.t. the situation of the more inclusive set up a. shown in fig. 30. In particular, the fraction of events without extra jets is about 30% and it's exceeded by the fraction of events with one additional jet, at the 40% level, at least for what concerns the ALPGEN S_1 and ALPGEN S_2 predictions. There are important fractions of events containing two and three extra jets, at the 20% and 10% level, respectively. From the lower panel, it can be noticed that the relative differences between the results of ALPGEN S_1 and ALPGEN S_2 and those of MC@NLO lie in a $\pm 20\%$ range for the predictions relative to the fraction of events with at least one extra jet.

4. Conclusions and perspectives

In this paper we presented a detailed phenomenological analysis of the EW and QCD contributions, as well as of their combination, to single W boson production in hadronic collisions, considering the energies of interest for the experiments at the Fermilab Tevatron and the CERN LHC and in the presence of realistic selection criteria. In our study, we made use of MC tools which include the recent advances in EW and QCD calculations.

We analyzed all the quantities of interest for the many facets of W physics programme at hadron colliders and showed that a far from trivial interplay between EW and QCD effects is present for most of the observables. We noticed, in particular, partial cancellations between EW and QCD corrections for the experimental distributions of interest for both precision studies (such as the luminosity monitoring or the measurement of the W mass) and searches for new physics. Remarkably, in the region of the high transverse mass tail above 1 TeV, important for the search for new gauge bosons, these cancellation occurs almost completely between huge positive QCD corrections and very large negative contributions due to EW Sudakov logarithms. This emphasizes the need for a careful combination of strong and EW contributions in present and future analyses of the CC DY

process, as also pointed out in [15] for the NC DY channel in the high invariant mass region at the LHC. We also remarked that the convolution of the EW effects with QCD shower evolution is definitely relevant for a correct simulation of the distributions, since the relative size and shape of EW contributions is considerably modified when compared with the same features in the absence of the combination with a QCD PS. This can be understood in terms of the modifications introduced by QCD PS on the kinematics of the final-state leptons w.r.t. a pure EW calculation. We also discussed in detail and evaluated the uncertainty inherent the combination of EW and QCD corrections by comparing different theoretical recipes (additive vs factorized) and showing that they can differ at a few per cent level.

In relation to the accuracy of the theoretical tools presently available and used by the experimental collaborations in comparison with the precision already reached at the Tevatron and foreseen at the LHC, some final comments are in order. While the predictions of the EW programs are in very good agreement and the situation can be considered well under control (also when taking into account multiple photon emission), the same can not be said, strictly speaking, for the QCD generators currently used in the experimental analyses at the Tevatron or for simulations by ATLAS and CMS collaborations. Actually, we noticed, for example, differences of 2% or more in predictions for the shape of the distributions relevant for W mass extraction between ResBos-A and our combination of EW and QCD tools. Therefore, it is our opinion that a cross-check of the Tevatron W mass results, generally obtained by means of ResBos in association with WGRAD or PHOTOS, with the predictions of our recipe, based on the combination of MC@NLO with HORACE, would be highly desirable, in view of a robust, high-precision measurement of M_W , which is such an important input for indirect constraints on the Higgs boson mass. On the other hand, we concluded that the results of the different QCD generators are in very good agreement for what concern the W rapidity and lepton pseudorapidity distributions, and that EW corrections are well under control for such distributions. This reinforces the need for deeper attempts to monitor the hadron collider luminosity with presently available tools in terms of such distributions, and this goal should be attainable at the Tevatron with a few per cent precision, a certainly useful “exercise” to pave the way to LHC collaborations for future luminosity measurements along this direction.

Concerning the forthcoming data taking at the LHC, we agree with the conclusions of [16, 17] about the feasibility of using the process-independent module PHOTOS to simulate photonic corrections around the W peak for early stages of data analysis, but we also provided clear evidences that such an approach to the treatment of EW corrections will not be sufficient in the later stages of analysis at high integrated luminosity. This caveat applies to high-precision extraction of the W boson properties at the LHC, as well as to predict correctly the SM background to new-physics searches in the high tail, where pure EW Sudakov logarithms and not photonic effects dominate within the full set of one-loop corrections. In particular, for such a region, two-loop Sudakov contributions and NNLO QCD corrections would be needed, together with the contribution of real W, Z emission.

In general, for the LHC we remarked that available calculations and tools do not currently allow to reach a theoretical accuracy better than some per cent level, when

excluding PDF uncertainties. If this could be acceptable for earlier stages of analysis, future measurements at the LHC would probably require the calculation of complete $\mathcal{O}(\alpha\alpha_s)$ corrections. All the necessary theoretical ingredients are not for the time being implemented into a single generator, which would represent the optimal solution for simulation and analysis of DY process in hadronic collisions, in its many and quite different aspects.

For readers' convenience, we summarize in a final Table the relative effects of the different sources of corrections to the integrated cross section. We also include a further Table reporting an *estimate* of the theoretical accuracy of the best predictions that combine QCD and EW corrections according to the different recipes proposed. In tab. 9 NLO QCD

$\delta(\%)$	NLO QCD	NLL QCD	NLO EW	Shower QCD	$\mathcal{O}(\alpha\alpha_s)$
Tevatron	8	16.8	-2.6	-1.3	~ 0.5
LHC a	-2	12.4	-2.6	1.4	~ 0.5
LHC b	21.8	20.9	-21.9	-0.6	~ 5

Table 9: Relative effect of the main sources of QCD, EW and mixed radiative corrections to the integrated cross sections for the Tevatron, LHC a and LHC b.

is the complete $\mathcal{O}(\alpha_s)$ correction, NLL QCD is the matrix element contribution of the NLO QCD correction, NLO EW is the full $\mathcal{O}(\alpha)$ correction, Shower QCD stands for the $\mathcal{O}(\alpha_s^n), n \geq 2$ correction and $\mathcal{O}(\alpha\alpha_s)$ represents the mixed EW-QCD corrections estimated by properly combining the additive and factorized cross sections. It is worth noticing in particular that the latter corrections remain below the 1% level for typical event selections at the Tevatron and the LHC, while they can amount to some per cent in the region important for new physics searches at the LHC.

$\delta(\%)$	$\delta\sigma/\sigma$ (scale)	$\delta\sigma/\sigma$ (FA)	$\delta\sigma/\sigma$
Tevatron	~ 1	~ 2	2
LHC a	~ 2.5	~ 2	2.5
LHC b	~ 1.5	~ 5	5

Table 10: Estimate of the present theoretical accuracy for the calculation of the integrated cross section at the Tevatron, LHC a and LHC b.

Concerning the theoretical accuracy of the integrated cross sections calculation shown in Tab. 10, it is a measure of the missing/incomplete higher order α_s^2 and $\alpha\alpha_s$ contributions. It has been assessed by neglecting the effect of the PDF uncertainties and according to the following procedure: the relative scale variation of the additive cross section $\delta\sigma/\sigma$ (scale) and the relative difference between the additive and factorized cross sections $\delta\sigma/\sigma$ (FA) have been computed and compared; as error estimate, the largest of the two entries has been taken.

Some comments are in order here. The above error estimate are in agreement with phenomenological results available in the literature about the size of NNLO QCD corrections, that are known to contribute at the $\sim 2\%$ level for standard cuts at the Tevatron and the

LHC. The errors quoted in Tab. 10 do not include the contributions of the two-loop EW Sudakov logarithms, that amount to a few per cent limited to the very high W transverse mass/lepton transverse momentum tails. Last, the error estimate reported can be considered as rather conservative. Actually, the factorized cross sections used in the present analysis contain the bulk of NNLO QCD contributions, as can be inferred by comparing the relative difference between the additive and factorized predictions with the exact results for NNLO corrections given in [38, 39, 40, 41] and finding them in pretty fine agreement. Hence, a more aggressive estimate of the theoretical error of the factorized formulae could be derived by taking the relative difference the factorized formulae, obtaining $O(1\%)$ at the Tevatron and the LHC a and $O(3\%)$ at LHC b. This estimate could be put on firmer grounds through detailed comparisons with the NNLO exact QCD calculations available in the literature. Furthermore, in the very hard tails of the distributions, the calculation of still unavailable $\alpha\alpha_s$ corrections should be performed.

Possible perspectives of the present work would be a careful analysis of how the precision measurement of the W boson mass and width is affected by the combination of EW and QCD corrections here proposed and an application of the same approach to the study of the NC DY channel.

Acknowledgments

We are indebted to all the colleagues who allowed us, with their invitations, to present preliminary results of our work at various conferences and workshops: M. Czakon, H. Czyz, G. Degrossi, S. Ferrag, S. Forte, J. Gluza, M. Grazzini, S. Jadach, W. Placzek, M. Srzypcek, D. Wackeroth, Z. Was and G. Zanderighi. We thank K. Ellis and J.M. Campbell for help with the use of the code MCFM and valuable correspondence, S. Frixione for helpful comments on the use of the code MC@NLO and M.L. Mangano for useful discussions and interest in our work. We acknowledge M.R. Whalley for help on LHAPDF. We are also grateful to the colleagues of the common paper [15] for fruitful collaboration. We wish to thank several experimental colleagues, in particular M. Bellomo, G. Polesello, A. Tricoli and V. Vercesi, for useful discussions and interest in our work. Useful discussions with P. Nason during the INFN Workshop on Monte Carlo's, Physics and Simulations at the LHC [100] are gratefully acknowledged.

The work of A. V. was supported by the European Community's Marie-Curie Research Training Network under contract MRTN-CT-2006-035505 (HEP-TOOLS).

References

- [1] D. Denegri, *Phys. Rept.* **403** (2004) 107 and references therein.
- [2] V.M. Abazov et al., CDF and DØ collaborations, *Phys. Rev.* **D 70** (2004) 092008, [hep-ex/0311039](#);
CDF Collaboration and DØ Collaboration, Combination of CDF and D0 results on the W boson mass and width, [arXiv:0808.0147 \[hep-ex\]](#);
T. Aaltonen et al., CDF Collaboration, *Phys. Rev.* **D 77** (2008) 112001, [arXiv:0708.3642 \[hep-ex\]](#).

- [3] D. Acosta et al., *Phys. Rev. D* **71** (2005) 052002, [hep-ex/0411059](#).
- [4] D. Acosta et al., *Phys. Rev. D* **71** (2005) 051104, [hep-ex/0501023](#).
- [5] U. Baur, Electroweak physics at the Tevatron and LHC: Theoretical status and perspectives, [hep-ph/0511064](#)
- [6] D. Wackeroth, Electroweak Physics: Theoretical Overview, [hep-ph/0610058](#)
- [7] S. Haywood et al., Electroweak Physics, in Proceedings of the Workshop on Standard Model Physics (and more) at the LHC, G. Altarelli and M.L. Mangano eds., CERN Report 2000-04, p. 117.
- [8] W.T. Giele and S. Keller, *Phys. Rev. D* **57** (1998) 4433, [hep-ph/9704419](#).
- [9] V. Büge, Ch. Jung, G. Quast, A. Ghezzi, M. Malberti, T. Tabarelli de Fatis, Prospects for the precision measurement of the W mass with the CMS detector at the LHC, CMS AN 20006/033;
N. Besson, M. Boonekamp, E. Klinkby, T. Petersen and S. Mehlhase, for ATLAS Collaboration, *Eur. Phys. J. C* **57** (2008) 627, [arXiv:0805.2093 \[hep-ex\]](#).
- [10] D. Froidevaux and V.A. Mitsou, Experimental prospects at the Large Hadron Collider, [arXiv:0905.0258 \[hep-ex\]](#).
- [11] M. Dittmar, F. Pauss and D. Zurcher, *Phys. Rev. D* **56** (1997) 7284, [hep-ex/9705004](#).
- [12] V.A. Khoze, A.D. Martin, R. Orava and M.G. Ryskin, *Eur. Phys. J. C* **19** (2001) 313, [hep-ph/0010163](#).
- [13] W.T. Giele and S.A. Keller, Hard scattering based luminosity measurement at hadron collider, [hep-ph/0104053](#).
- [14] G. Polesello and M. Prata, *Eur. Phys. J. C* **32S2** (2003) 55.
- [15] C. Buttar et al., Standard Model Handles and Candles Working Group: Tools and Jets Summary Report, Les Houches 2007, Physics at TeV colliders, [arXiv:0803.0678 \[hep-ph\]](#).
- [16] N. E. Adam, V. Halyo, S. A. Yost and W. Zhu, *J. High Energy Phys.* **0809** (2008) 133, [arXiv:0808.0758 \[hep-ph\]](#).
- [17] N. E. Adam, V. Halyo and S. A. Yost, *J. High Energy Phys.* **0805** (2008) 062, [arXiv:0802.3251 \[hep-ph\]](#).
- [18] G. Balossini et al., *J. Phys. Conf. Ser.* **110** (2008) 042002;
G. Balossini et al., *Acta Phys. Polon. B* **39** (2008) 1675, [arXiv:0805.1129 \[hep-ph\]](#);
G. Balossini et al., *Acta Phys. Polon. B* **38** (2007) 3407.
- [19] D. Wackeroth and W. Hollik, *Phys. Rev. D* **55** (1997) 6788, [hep-ph/9606398](#).
- [20] U. Baur, S. Keller and D. Wackeroth, *Phys. Rev. D* **59** (1999) 013002, [hep-ph/9807417](#).
- [21] S. Dittmaier and M. Krämer, *Phys. Rev. D* **65** (2002) 073007, [hep-ph/0109062](#).
- [22] U. Baur and D. Wackeroth, *Phys. Rev. D* **70** (2004) 073015, [hep-ph/0405191](#).
- [23] V. A. Zykunov, *Eur. Phys. J. Direct. C* **3** (2001) 9, [hep-ph/0107059](#);
V. A. Zykunov, *Phys. Atom. Nucl.* **71** (2008) 732;
V. A. Zykunov, *Phys. Atom. Nucl.* **69** (2006) 1522.

- [24] A. Arbuzov, D. Bardin, S. Bondarenko, P. Christova, L. Kalinovskaya, G. Nanava and R. Sadykov, *Eur. Phys. J. C* **46** (2006) 407, [hep-ph/0506110](#).
- [25] C.M. Carloni Calame, G. Montagna, O. Nicrosini and A. Vicini, *J. High Energy Phys.* **12** (2006) 016, [hep-ph/0609170](#).
- [26] S. Brensing, S. Dittmaier, M. 1. Kramer and A. Muck, *Phys. Rev. D* **77** (2008) 073006, [arXiv:0710.3309 \[hep-ph\]](#).
- [27] C. Buttar et al., Les houches physics at TeV colliders 2005, standard model and Higgs working group: Summary report, [hep-ph/0604120](#).
- [28] C.E. Gerber et al., Tevatron-for-LHC Report: Top and Electroweak Physics, [arXiv:0705.3251 \[hep-ph\]](#).
- [29] C. M. Carloni Calame, G. Montagna, O. Nicrosini and M. Treccani, *Phys. Rev. D* **69** (2004) 037301, [hep-ph/0303102](#).
- [30] C. M. Carloni Calame, G. Montagna, O. Nicrosini and M. Treccani, *J. High Energy Phys.* **0505** (2006) 019, [hep-ph/0502218](#)
- [31] W. Placzek and S. Jadach, *Eur. Phys. J. C* **29** (2003) 325, [hep-ph/0302065](#).
- [32] P. Golonka and Z. Was, *Eur. Phys. J. C* **45** (2006) 97, [hep-ph/0506026](#).
- [33] K. Hamilton and P. Richardson, *J. High Energy Phys.* **0607** (2006) 010, [hep-ph/0603034](#).
- [34] C.M. Carloni Calame, S. Jadach, G. Montagna, O. Nicrosini and W. Placzek, *Acta Phys. Polon. B* **35** (2004) 1643, [hep-ph/0402235](#).
- [35] G. Altarelli, R. K. Ellis and G. Martinelli, *Nucl. Phys. B* **157** (1979) 461.
- [36] R. Hamberg, W. L. van Neerven and T. Matsuura, *Nucl. Phys. B Nucl. Phys. B* **359** (1991) 343 [Erratum *ibid.* **644** (2002) 403].
- [37] J. M. Campbell and R. K. Ellis, *Phys. Rev. D* **65**, 113007 (2002), [hep-ph/0202176](#);
J. M. Campbell and R. K. Ellis, *Phys. Rev. D* **62**, 114012 (2000), [hep-ph/0006304](#);
J. M. Campbell and R. K. Ellis, *Phys. Rev. D* **60**, 113006 (1999), [hep-ph/9905386](#).
- [38] C. Anastasiou, L. J. Dixon, K. Melnikov and F. Petriello, *Phys. Rev. Lett.* **91** (2003) 182002, [hep-ph/0306192](#).
- [39] C. Anastasiou, L. J. Dixon, K. Melnikov and F. Petriello, *Phys. Rev. D* **69** (2004) 094008, [hep-ph/0312266](#).
- [40] K. Melnikov and F. Petriello, *Phys. Rev. Lett.* **96** (2006) 231803, [hep-ph/0603182](#).
- [41] K. Melnikov and F. Petriello, *Phys. Rev. D* **74** (2006) 114017, [hep-ph/0609070](#).
- [42] S. Catani, L. Cieri, G. Ferrera, D. de Florian, M. Grazzini, Vector boson production at hadron colliders: a fully exclusive QCD calculation at NNLO, [arXiv:0903.2120 \[hep-ph\]](#), *Phys. Rev. Lett.* **103** (2009) 082001.
- [43] C. Balazs and C. P. Yuan, *Phys. Rev. D* **56** (1997) 5558, [hep-ph/9704258](#).
- [44] F. Landry, R. Brock, P.M. Nadolsky and C.-P. Yuan, *Phys. Rev. D* **67** (2003) 073016, [hep-ph/0212159](#).
- [45] S. Frixione and B. R. Webber, *J. High Energy Phys.* **0206** (2002) 029, [hep-ph/0204244](#).

- [46] P. Nason, *J. High Energy Phys.* **0411** (2004) 040, [hep-ph/0409146](#);
S. Frixione, P. Nason and C. Oleari, *J. High Energy Phys.* **0711** (2007) 070,
[arXiv:0709.2092 \[hep-ph\]](#).
- [47] S. Alioli, P. Nason, C. Oleari and E. Re, *J. High Energy Phys.* **0807** (2008) 060,
[arXiv:0805.4802 \[hep-ph\]](#).
- [48] M.L. Mangano, M. Moretti, F. Piccinini, R. Pittau and A.D. Polosa, *J. High Energy Phys.* **0307** (2003) 001, [hep-ph/0206293](#).
- [49] A. Schalicke and F. Krauss, *J. High Energy Phys.* **0507** (2005) 018, [hep-ph/0503281](#);
T. Gleisberg et. al., *J. High Energy Phys.* **0402** (2004) 056, [hep-ph/0311263](#);
T. Gleisberg et al., *J. High Energy Phys.* **0902** (2009) 007, [arXiv:0811.4622 \[hep-ph\]](#).
- [50] T. Stelzer and W.F. Long, *Comput. Phys. Commun.* **81** (1994) 357, [hep-ph/9401258](#);
F. Maltoni and T. Stelzer, *J. High Energy Phys.* **02** (2003) 02, [hep-ph/0208156](#);
J. Alwall et. al., *J. High Energy Phys.* **0709** (2007) 028, [arXiv:0706.2334 \[hep-ph\]](#).
- [51] A. Kanaki and C. G. Papadopoulos, *Comput. Phys. Commun.* **132** (2000) 306;
A. Cafarella, C. G. Papadopoulos and M. Worek, *Comput. Phys. Commun.* **180** (2009) 1941.
- [52] P.M. Nadolsky, *AIP Conf.Proc.* **753** (2005) 158, [hep-ph/0412146](#).
- [53] U. Baur, *Int. J. Mod. Phys. E* **17** (2008) 826, [hep-ph/0701164](#).
- [54] P.Z. Skands, *AIP Conf. Proc.* **792** (2005) 73, [hep-ph/0507129](#).
- [55] D.A. Kosower, *AIP Conf. Proc.* **842** (2006) 189, [hep-ph/0604015](#)
- [56] Q.-H. Cao and C.-P. Yuan, *Phys. Rev. Lett.* **93** (2004) 042001, [hep-ph/0401026](#).
- [57] S. Jadach, M. Skrzypek, P. Stephens, Z. Was and W. Placzek, *Acta Phys. Polon. B* **38**
(2007) 2305.
- [58] S. Frixione and M.L. Mangano, *J. High Energy Phys.* **05** (2004) 056, [hep-ph/0405130](#).
- [59] H. Jung et al., Proceedings of the workshop: HERA and the LHC workshop series on the
implications of HERA for LHC physics, [arXiv:0903.3861 \[hep-ph\]](#);
S. Alekhin et al., HERA and the LHC: A Workshop on the implications of HERA for LHC
physics: Proceedings Part A and Part B, [hep-ph/0601012](#) and [hep-ph/0601013](#).
- [60] R.S. Thorne, A.D. Martin, R.G. Roberts and W.J. Stirling, *AIP Conf. Proc.* **792** (2005) 365,
[hep-ph/0507015](#).
- [61] M.R. Whalley, D. Bourikov, R.C. Group, The Les Houches accord PDFs (LHAPDF) and
LHAGLUE, [hep-ph/0508110](#).
- [62] A.D. Martin, R.G. Roberts, W.J. Stirling and R.S. Thorne, *Eur. Phys. J. C* **28** (2003) 455,
[hep-ph/0211080](#).
- [63] J. Pumplin, D.R. Stump, J. Huston, H.L. Lai, P. Nadolsky and W.K. Tung, *J. High Energy
Phys.* **0207** (2002) 012, [hep-ph/0201195](#);
D. Stump, J. Huston, J. Pumplin, W. K. Tung, H. L. Lai, S. Kuhlmann and J. F. Owens, *J.
High Energy Phys.* **0310** (2003) 046, [hep-ph/0303013](#).
- [64] A. Tricoli, A. Cooper-Sarkar and C. Gwenlan, Uncertainties on W and Z production at the
LHC, [hep-ex/0509002](#)

- [65] A.D. Martin, R.G. Roberts, W.J. Stirling and R.S. Thorne, *Eur. Phys. J. C* **35** (2004) 325, [hep-ph/0308087](#).
- [66] J. Huston, J. Pumplin, D.R. Stump and W.K. Tung, *J. High Energy Phys.* **0506** (2005) 080, [hep-ph/0502080](#).
- [67] A. D. Martin, R. G. Roberts, W. J. Stirling and R. S. Thorne, *Eur. Phys. J. C* **39** (2005) 155, [hep-ph/0411040](#).
- [68] M. Roth and S. Weinzierl, *Phys. Lett. B* **590** (2004) 190, [hep-ph/0403200](#).
- [69] H. Spiesberger, *Phys. Rev. D* **52** (1995) 4936, [hep-ph/9412286](#).
- [70] J. Kripfganz and H. Perlt, *Z. Physik C* **41** (1988) 319.
- [71] A.D. Martin, W.J. Stirling, R.S. Thorne, G. Watt, *Phys. Lett. B* **652** (2007) 292, [arXiv:0901.0002 \[hep-ph\]](#).
- [72] P. M. Nadolsky et al., *Phys. Rev. D* **D78** (2008) 013004, [[arXiv:0802.0007 \[hep-ph\]](#)].
- [73] R.S. Thorne, A.D. Martin, W.J. Stirling, G. Watt, [arXiv:0907.2387 \[hep-ph\]](#).
- [74] G. Corcella et al., HERWIG 6.5 release note, [hep-ph/0210213](#).
- [75] T. Sjöstrand, P. Eden, C. Friberg, L. Lönnblad, G. Miu, S. Mrenna and E. Norrbin, *Comput. Phys. Commun.* **135** (2001) 238, [hep-ph/0010017](#).
- [76] R. Kuhn, F. Krauss, B. Ivanyi and G. Soff, *Comput. Phys. Commun.* **134** (2001) 223, [hep-ph/0004270](#);
F. Krauss, A. Schälicke and G. Soff, *Comput. Phys. Commun.* **174** (2006) 876, [hep-ph/0503087](#).
- [77] S. Gieseke, P. Stephens and B. Webber, *J. High Energy Phys.* **12** (2003) 045, [hep-ph/0310083](#).
- [78] T. Sjöstrand and P. Skands, *Eur. Phys. J. C* **39** (2005) 129, [hep-ph/0408302](#);
T. Sjöstran, S. Mrenna and P. Skands, *Comput. Phys. Commun.* **178** (2008) 852, [arXiv:0710.3820 \[hep-ph\]](#).
- [79] F. Caravaglios and M. Moretti, *Phys. Lett. B* **358** (1995) 332, [hep-ph/9507237](#);
F. Caravaglios, M.L. Mangano, M. Moretti and R. Pittau, *Nucl. Phys. B* **539** (1999) 215, [hep-ph/9807570](#).
- [80] S. Catani, F. Krauss, R. Kuhn and B.R. Webber. *J. High Energy Phys.* **11** (2001) 063, [hep-ph/0109231](#).
- [81] L. Lönnblad, *J. High Energy Phys.* **05** (2002) 046, [hep-ph/0112284](#).
- [82] M. Mangano, The so-called MLM prescription for ME/PS matching , talk given at the Fermilab ME/MC Tuning Workshop, October, 2004.
- [83] S. Mrenna and P. Richardson, *J. High Energy Phys.* **05** (2004) 040, [hep-ph/0312274](#).
- [84] M.L. Mangano, M. Moretti, F. Piccinini and M. Treccani, *J. High Energy Phys.* **01** (2007) 013, [hep-ph/0611129](#).
- [85] S. Höche et al, Matching parton showers and matrix elements, [hep-ph/0602031](#).
- [86] J. Alwall et al., *Eur. Phys. J. C* **53** (2008) 473, [arXiv:0706.2569 \[hep-ph\]](#).
- [87] J.C. Collins, D.E. Soper and G. Sterman, *Nucl. Phys. B* **250** (1985) 199.

- [88] K.-P. O. Diener, S. Dittmaier and W. Hollik, *Phys. Rev. D* **72** (2005) 093003, [hep-ph/0509084](#).
- [89] W. Hollik, T. Kasprzik and B. A. Kniehl, *Nucl. Phys. B* **790** (2008) 138, [arXiv:0707.2553 \[hep-ph\]](#).
- [90] J. H. Kuhn, A. Kulesza, S. Pozzorini and M. Schulze, *Nucl. Phys. B* **797** (2008) 27, [arXiv:0708.0476 \[hep-ph\]](#);
J. H. Kuhn, A. Kulesza, S. Pozzorini and M. Schulze, *Phys. Lett. B* **651** (2007) 160, [hep-ph/0703283](#).
- [91] A. Denner, S. Dittmaier, T. Kasprzik and A. Muck, Electroweak corrections to $W + \text{jet}$ hadroproduction including leptonic W -boson decays, [arXiv:0906.1656 \[hep-ph\]](#).
- [92] E. Maina, S. Moretti and D. A. Ross, *Phys. Lett. B* **593** (2004) 143 [Erratum-ibid. B **614** (2005) 216], [hep-ph/0403050](#).
- [93] P.M. Nadolsky and Z. Sullivan, PDF uncertainties in WH production at Tevatron, [hep-ph/0110378](#).
- [94] S. Catani and B. R. Webber, *JHEP* **9710** (1997) 005 [[arXiv:hep-ph/9710333](#)] and references therein.
- [95] U. Baur, *Phys. Rev. D* **75** (2007) 013005, [hep-ph/0611241](#)
- [96] A. Denner, B. Jantzen and S. Pozzorini, *Nucl. Phys. B* **761** (2007) 1, [hep-ph/0608326](#).
- [97] B. Jantzen, J. H. Kuhn, A. A. Penin and V. A. Smirnov, *Nucl. Phys. B* **731** (2005) 188 [Erratum-ibid. B **752** (2006) 327], [hep-ph/0509157](#).
- [98] B. Jantzen, J. H. Kuhn, A. A. Penin and V. A. Smirnov, *Phys. Rev. D* **72** (2005) 051301 [Erratum-ibid. D **74** (2006) 019901], [hep-ph/0504111](#).
- [99] F.E. Paige and S.D. Protopopescu, in *Physics of the SSC, Snowmass, 1986, Colorado*, edited by R. Donaldson and J. Marx.
- [100] F. Ambroglini et al., *Proceedings of the Workshop on Monte Carlo's, Physics and Simulations at the LHC PART I*, [arXiv:0902.0293 \[hep-ph\]](#);
F. Ambroglini et al., *Proceedings of the Workshop on Monte Carlo's, Physics and Simulations at the LHC PART II*, [arXiv:0902.0180 \[hep-ph\]](#).